SCIENCE CHINA
Physics, Mechanics & Astronomy

CrossMark click for updates

•Invited Review•
Special Topic: Quantum Materials and Intelligent Devices

November 2023 Vol. 66 No. 11: 117502
https://doi.org/10.1007/s11433-022-1989-9

Controllable growth of two-dimensional quantum materials

Xin Sui[1†], Zhibin Zhang[2,3†*], and Kaihui Liu[1,2,3*]

[1] *International Centre for Quantum Materials, Collaborative Innovation Centre of Quantum Matter, Peking University, Beijing 100871, China;*
[2] *State Key Laboratory for Mesoscopic Physics, Frontiers Science Centre for Nano-optoelectronics, School of Physics, Peking University, Beijing 100871, China;*
[3] *Songshan Lake Materials Laboratory, Institute of Physics, Chinese Academy of Sciences, Dongguan 523808, China*

Received June 30, 2022; accepted September 1, 2022; published online April 18, 2023

Two-dimensional (2D) quantum materials have attracted extensive attention due to their superior properties at the atomic thickness. Numerous novel physical phenomena, including the quantum Hall effect, fractional quantum Hall effect, quantum anomalous Hall effect and topological superconductor phase or topological insulator phase, have been discovered on different 2D quantum materials. Over the past decades, various technologies have been developed to prepare the 2D quantum materials and all of them have demonstrated their specific advantages. In this review, we comprehensively summarize the commonly used growth methods for the 2D quantum materials and discuss the corresponding controllable growth strategies. Finally, we provide a summary and a perspective for future studies.

2D quantum material, controllable growth, growth methods

PACS number(s): 68.55.Jk, 74.62.Bf, 81.10.-h, 81.15.-z, 81.20.-n

Citation: X. Sui, Z. Zhang, and K. Liu, Controllable growth of two-dimensional quantum materials, Sci. China-Phys. Mech. Astron. **66**, 117502 (2023), https://doi.org/10.1007/s11433-022-1989-9

1 Introduction

In the course of human history, material science has played an important role in the development of technology, from the Stone Age to the Bronze Age, until the silicon-based material age in the 20th century and the new material age in the 21st century. Among all the new materials, 2D quantum materials have been considered to be a promising candidate for the innovation of next-generation new technology, mainly due to their extreme thickness [1-3] (typically down to the atomic thick, which could in principle realize the fabrication of ultrasmall devices), excellent properties like ultrahigh mobility [4], ultrafast charge transfer [5] and high thermal conductivity [6] (which is crucial for high-speed devices), full components including the conductor [7], semiconductor [8-10], insulator [11,12] and magnet [13-16] (which could construct full 2D quantum devices) and the compatibility with state-of-the-art silicon-based processing techniques (which is essential for future massive industrial applications) [17-19]. Because of these advances, 2D quantum materials have demonstrated great potential in the application of electronics [20,21], optoelectronics [22,23], optics [24,25], magnetics [26,27] and catalysis [28]. Generally, to realize these appealing applications, the controllable growth of 2D quantum materials is a prerequisite [29].

Since the first successful mechanical exfoliation of graphene in 2004 [7], various methods on how to realize the controllable growth of 2D quantum materials emerged in an endless stream, every with its own advantages. In this re-

*Corresponding authors (Kaihui Liu, email: khliu@pku.edu.cn; Zhibin Zhang, email: zhibinzhang@pku.edu.cn)
†These authors contributed equally to this work.

© Science China Press 2023

view, we summarize some of these typical synthesis methods (Figure 1), including exfoliation, molecular beam epitaxy (MBE), atomic layer deposition (ALD), physical vapor deposition (PVD), chemical vapor transport (CVT) and chemical vapor deposition (CVD). We systemically discuss their histories, growth principles, advantages and disadvantages, scopes of applications and other characteristics. Finally, we give a summary and an outlook.

2 Exfoliation

Exfoliation is a typical "Top-down" method to obtain mono- and multi-layer 2D quantum materials, which applied an external force on the bulk materials to destroy the weak van der Waals (vdW) interlayer force [30,31]. This external force can be realized in many forms and the most typical and famous one is using a Scotch tape. In 2004, Novoselov et al. [7] produced the first graphene flake by applying a tape to the bulk highly oriented pyrolytic graphite (HOPG) surface. Their pioneering work initiated the vigorous research toward 2D quantum materials.

In 2008, Hernandez et al. [32] found that large-yield graphene can be prepared by the sonication-assisted liquid-phase exfoliation method. This method has been rapidly developed and become a major strategy for the mass production of graphene. In 2010, Zhao et al. [33] demonstrated a feasible way to produce graphene from graphite using wet ball milling exfoliation. In the meantime, Knieke et al. [34] also reported that the free-standing and highly dispersed mono- and multilayer graphene sheets can be directly dispersed under a simple wet grinding process at ambient temperature. Apart from the liquid-phase exfoliation, dry milling [35] can be also used for producing a large quantity of graphene. For example, Lin et al. [36] reported a sulfur-assisted exfoliation of graphite and they obtained the graphene-sulfur composites and freestanding low-defect graphene sheets in 2013.

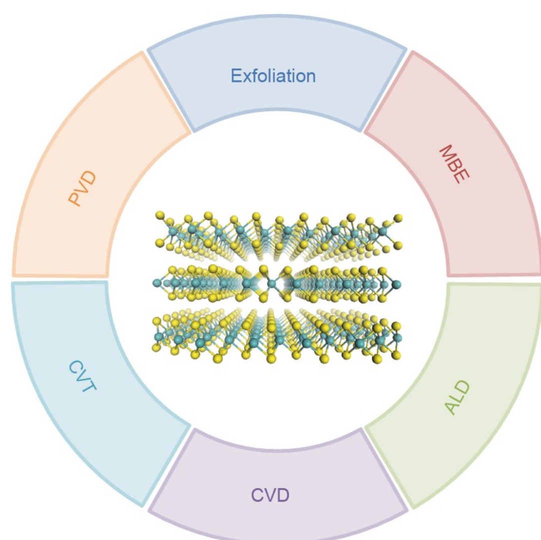

Figure 1 (Color online) Different methods for the controllable growth of 2D quantum materials.

In principle, the liquid exfoliation and milling method are effective in the mass production of 2D flakes, while they show limits in the control of quality. The mechanical exfoliation method is a powerful way to prepare high-quality 2D flakes, however, its layer control and large-scale uniformity remain great challenges. Recently, many modified mechanical exfoliation methods have been developed to address the layer control and uniformity issues [37-39].

Many groups have found that by selecting a suitable substrate, the external force can be provided to assist the mechanical exfoliation process. For example, the interlayer bonding of Fe_3GeTe_2 (FGT, a ferromagnetism material) is not strong enough for thin flakes of reasonable size (about 5 μm) to survive conventional mechanical exfoliation processes. In 2018, Deng et al. [14] developed an Al_2O_3-assisted exfoliation method to isolate FGT monolayers (Figure 2(a)). First, they used Al_2O_3 thin film to cover the FGT bulk crystal. Then they picked up the Al_2O_3 film with a thermal release tape. The Al_2O_3/FGT stack was then released by heating onto a piece of polydimethylsiloxane (PDMS). Next, they stamped the PDMS/FGT/Al_2O_3 onto a substrate and quickly peeled off the PDMS. The FGT flakes covered with Al_2O_3 film were left on the substrate. Figure 2(d) shows an optical image of 1-3 layer FGT flakes on Al_2O_3 film. And the 0.8 nm steps in the height profile match the FGT monolayer thickness (Figure 2(e) and (f)), which means that they have successfully prepared the large monolayer FGT flakes for further investigations. They demonstrated that this method is not only applicable to FET but also generalized to other 2D quantum materials, and could facilitate the exfoliation of various 2D quantum materials.

Recent research found that Au is promising for the high-yield exfoliation of many 2D quantum materials [40], because Au has not only a strong interaction with group 16 chalcogens and 17 halogens but also a low chemical reactivity and air stability. According to that, Huang et al. [41] identified an Au-assisted exfoliation method that underpins a universal route for producing large-area monolayers. The Au-assisted exfoliation process is shown in Figure 2(b). They applied gentle pressure to make good contact between the layered bulk crystal and Au, and the adhesive tape was placed on the outward side of the crystal. Next, they peeled off the tape to remove the major portion of the crystal. Then one or few large-area monolayer flakes would be left on the Au surface. As a result, they isolated 40 types of single-crystal monolayers, including MoS_2, BP, $CrSiTe_3$ and $PtSe_2$ as shown in Figure 2(g)-(j). Most of the obtained monolayers are with millimeter-size and high-quality. The Au-assisted mechanical exfoliation method can also be used in transition

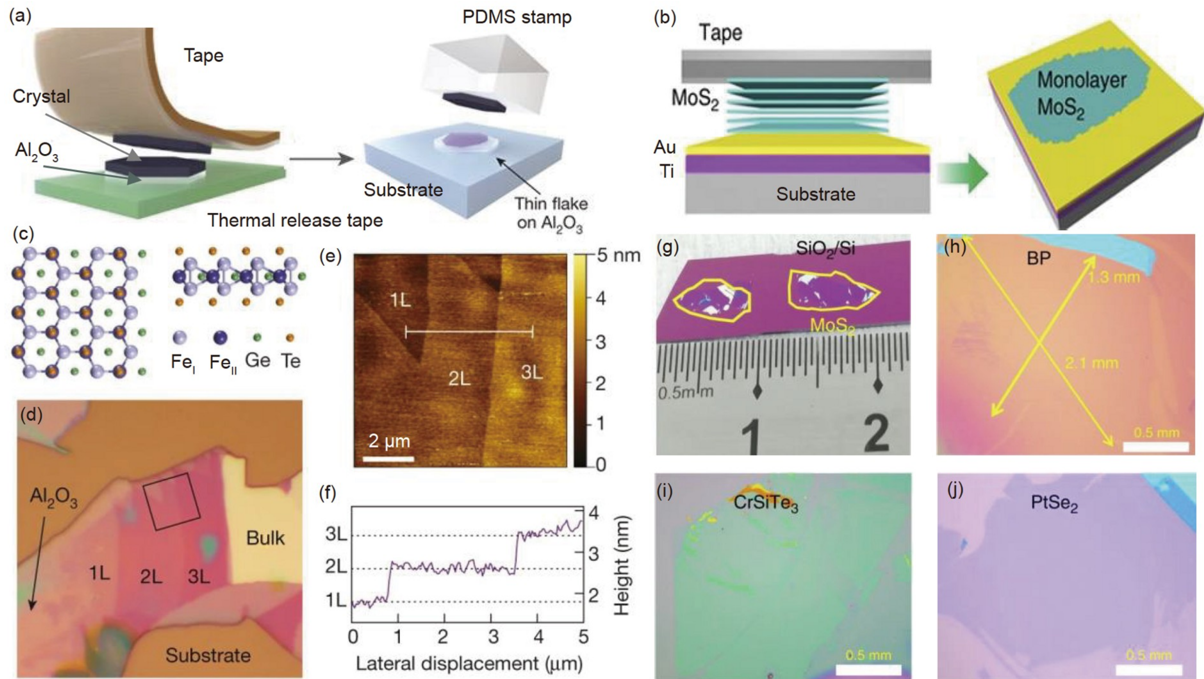

Figure 2 (Color online) Substrate-assisted mechanical exfoliation method. (a) Al_2O_3-assisted mechanical exfoliation method; (b) Au-assisted mechanical exfoliation method; (c) atomic structure of monolayer FGT; (d) optical image of 1-3 layer exfoliated FGT flakes on Al_2O_3; (e) atomic force microscopy (AFM) image of the marked area in (d); (f) cross-sectional profile of the FGT flakes along the white line in (e); (g) optical image of exfoliated MoS_2 on SiO_2/Si; (h)-(j) optical images of exfoliated BP, $CrSiTe_3$ and $PtSe_2$. (a), (c)-(f) Reproduced with permission from ref. [14]. Copyright©Springer Nature. (b), (g)-(i) Reproduced with permission from ref. [41]. Copyright©Springer Nature.

metal dichalcogenides (TMDs) [42,43].

The production of graphene by exfoliation has triggered the exploration of 2D quantum materials. By choosing a suitable substrate, the size and the quality of the product can be sufficiently improved [44-47]. In the past decades, exfoliation has been one of the most powerful methods for the preparation of 2D quantum materials and it has also played an important role in the exploration of the physical and chemical properties of 2D quantum materials [48,49].

3 Molecular-beam epitaxy method (MBE)

MBE is an epitaxial growth technique of thin films which involves the reaction of one or several thermal molecular beams on a crystalline surface under ultra-high vacuum conditions [50]. MBE was first developed at IBM and Bell Laboratories in the 1960s. In 1968, Arthur Jr. [51] first reported the epitaxy of GaAs thin films using separate “molecular beam” of gallium and arsenic. Alfred Y. Cho and collaborators jointly developed the technique that we call MBE today [52]. Firms like Riber introduced the first off-the-shelf MBE systems in the 1980s, driving the modernization of MBE [53].

In a typical MBE process, the solid source is slowly sublimated by heating, and then the gaseous substances react on the surface of the substrate to realize the epitaxial growth process. What is more, every MBE equipment is generally equipped with the reflection high-energy electron diffraction (RHEED) system for the *in-situ* characterization of the crystal growth process (Figure 3(a)).

MBE plays a key role in material synthesis since its development. For the fabrication of 2D materials, MBE method also has several natural advantages, such as (1) the ultra-high vacuum (UHV) environment. Some 2D monoelemental materials (also known as Xenes), like silicene [54] and borophene [55] were firstly fabricated in experiments through epitaxial growth in UHV environment. In 2015, Zhu et al. [56] reported the successful fabrication of 2D stanene (Figure 3(b)) by MBE firstly, confirmed by atomic and electronic characterizations. (2) The *in-situ* characterization ability allowing one to precisely control the sample's quality. Ji et al. [57] synthesized and transferred freestanding perovskite oxide films down to the thickness of one unit cell through MBE (Figure 3(c)). Ugeda et al. [58] synthesized monolayer $NbSe_2$ by MBE technology (Figure 3(d)) and demonstrated that the 3 × 3 charge density wave (CDW) order in $NbSe_2$ remains intact in two dimensions. Zhang et al. [59] also reported the growth of Bi_2Se_3 films with various thicknesses using MBE method and found that the energy gap opening can be clearly seen when the thickness is below six quintuple layers (Figure 3(e)). (3) The control of the solid source, which provides extra freedoms for the synthesis of 2D quantum materials. Zhao et al. [60] showed the self-

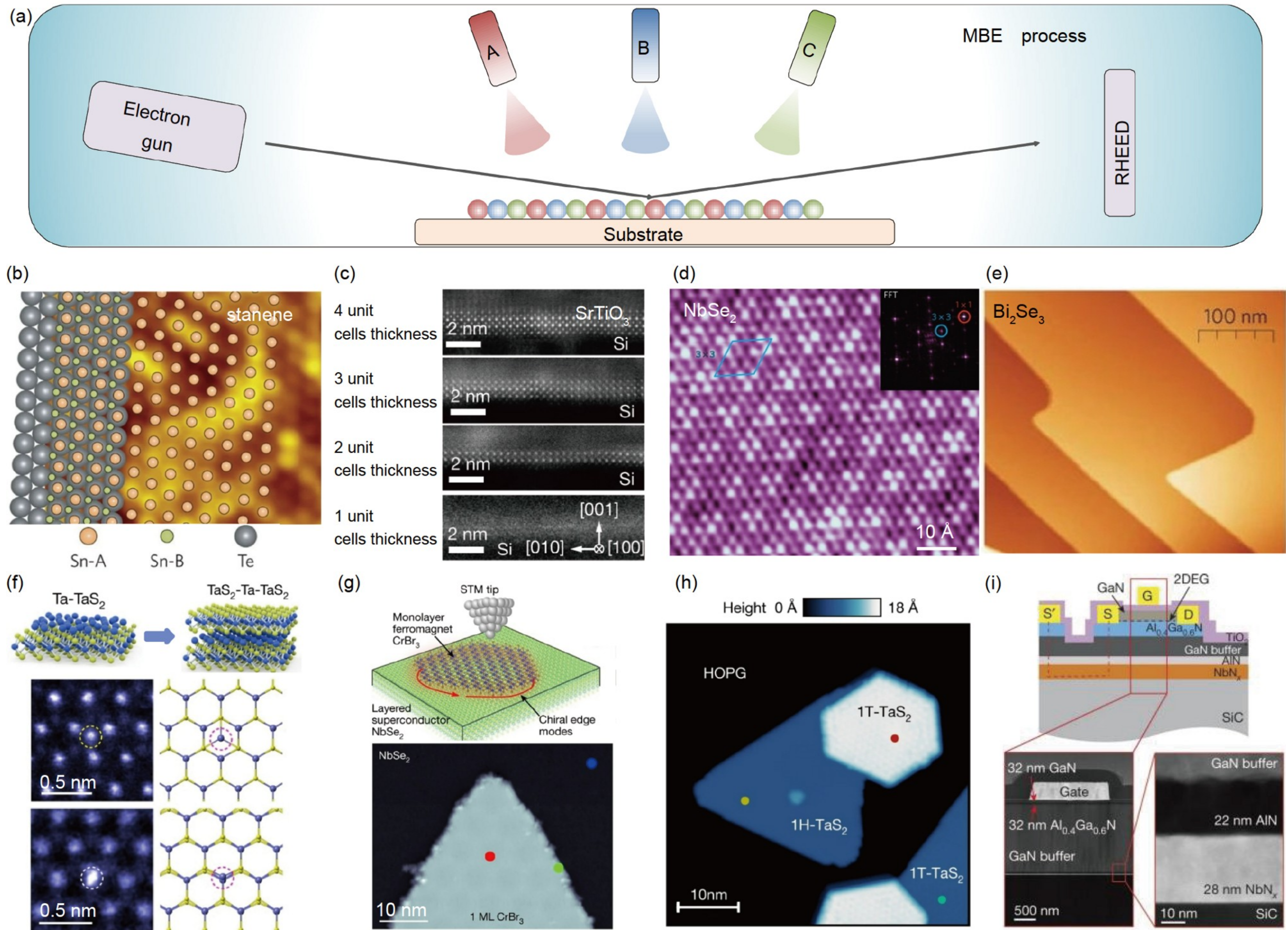

Figure 3 (Color online) Molecular-beam epitaxy method. (a) The schematic diagram of MBE process; (b) atomic structure model for the 2D stanene on Bi_2Te_3(111); (c) cross-sectional high-angle annular dark-field images of ultrathin $SrTiO_3$(STO) films of various unit-cell thicknesses; (d) atomically resolved scanning tunnelling microscopy (STM) image and fast fourier transform (FFT) of single-layer $NbSe_2$ at 5 K; (e) STM image of the 50 quintuple layer Bi_2Se_3. (f) Top: schematic diagram of the self-intercalated 2D crystals; down: atomic-resolution scanning transmission electron microscopy-annular dark field (STEM-ADF) image of monolayer TaS_2 with different configurations. (g) Top: schematic of the $CrBr_3$-$NbSe_2$ heterostructures experimental set-up; down: STM image of a monolayer $CrBr_3$ island on $NbSe_2$. (h) STM image of a 1T/1H-TaS_2 vertical heterostructure on HOPG; (i) cross-section schematic (top) and STEM image (bottom left and right) of Al(Ga)N/GaN HEMTs/NbN_x on SiC. (b)-(i) Reproduced with permission from refs. [56-63], respectively. Copyright©Springer Nature.

intercalation of Ta into bilayer transition TaS_2 during growth, and they synthesized a class of ultrathin, covalently bonded materials by controlling the flux ratio of Ta and S (Figure 3(f)). (4) The versatile compatibility, providing opportunities for the synthesis of vdW heterostructures through the choice of suitable solid source and substrate. Kezilebieke et al. [61] fabricated vdW heterostructures that combine a 2D ferromagnet with a superconductor, and observed 2D topological superconductivity in the system (Figure 3(g)). Vaňo et al. [62] realized an artificial vdW heterostructure of 1H/1T-TaS_2 hosting heavy-fermion properties (Figure 3(h)). Yan et al. [63] grew an AlGaN/GaN quantum-well heterostructure directly on the top of NbN superconductor by MBE (Figure 3(i)), combining the quantum effects with the excellent properties of semiconductors.

The birth and development of MBE technology are of significant importance in the progress of material science. Novel physical phenomena like fractional quantum Hall effect [64], quantum spin Hall effect [65], quantum anomalous effect [66] and topological superconductivity [61] were discovered in materials fabricated by MBE. The advantages of *in-situ* characterization and high-purity of MBE method are attractive for the preparation of current 2D quantum materials.

4 Atomic layer deposition method (ALD)

ALD is a thin-film deposition technique based on the sequential use of a gas-phase chemical process. Before 2000, this technology was called atomic layer epitaxy (ALE) [67], and later it was called ALD because most films grown using sequential, self-limiting surface reactions were not epitaxial to the underlying substrates [68]. ALD or ALE was devel-

oped in Finland in the 1970s. Tuomo Suntola, the pioneer of ALE, prepared ZnS using the primary version of ALE technology in 1974. He then applied for an ALE patent in 1977 [68] and published the first literature on ALE about ZnTe in 1980 [69]. Later in 1988, Microchemistry sold the first commercial ALE reactor F-120 [68].

ALD could be used to grow the atomic-scale films owing to the self-limiting surface reactions on the surface of the substrate. At the beginning of the ALD process, the surface is covered by ligands. The alternating precursors are introduced as a series of sequential, non-overlapping pulses. In each pulse, the precursor molecule reacts with the surface in a self-limiting way. When all of the reactive sites on the substrate are consumed, the reaction terminates (Figure 4(a) [70-75]). After an ALD cycle, the ligands on the surface are similar, so the deposition process can be cycled [76,77]. By changing the number of cycles, the experimenters can control the thickness of the thin film to the Ångstrom or monolayer level. Besides, ALD can fabricate materials uniformly with high precision on complex and large substrates at a low temperature.

A variety of 2D quantum materials including graphene [70], hexagonal boron nitride (h-BN) [78,79], TMDS [80,81] and group IIIA-VA metal chalcogenides [82] have been synthesized by ALD. Zhang et al. [70] prepared large graphene sheets with excellent quality at a growth temperature as low as 400°C (Figure 4(b)). Park et al. [71] developed micrometer-scale and wafer-scale WS_2 on SiO_2 (Figure 4(c)). By changing the cycling number, Tan et al. [72] realized the growth of mono- to multilayer thick MoS_2 film on a sapphire wafer substrate at 300°C (Figure 4(d)).

Reactive ligands on the substrate surface are the keys to the ALD process. Wang et al. [73] obtained a uniform ultrathin ALD coating on perylene tetracarboxylic acid (PTCA) functionalizing graphene surface (Figure 4(e)). This method can selectively introduce densely packed surface groups on graphene. In addition, ALD technology can also realize the directional deposition of substances on the surface of the substrate. Kim et al. [74] used ALD to deposit Pt predominantly on the grain boundaries, folds and cracks of

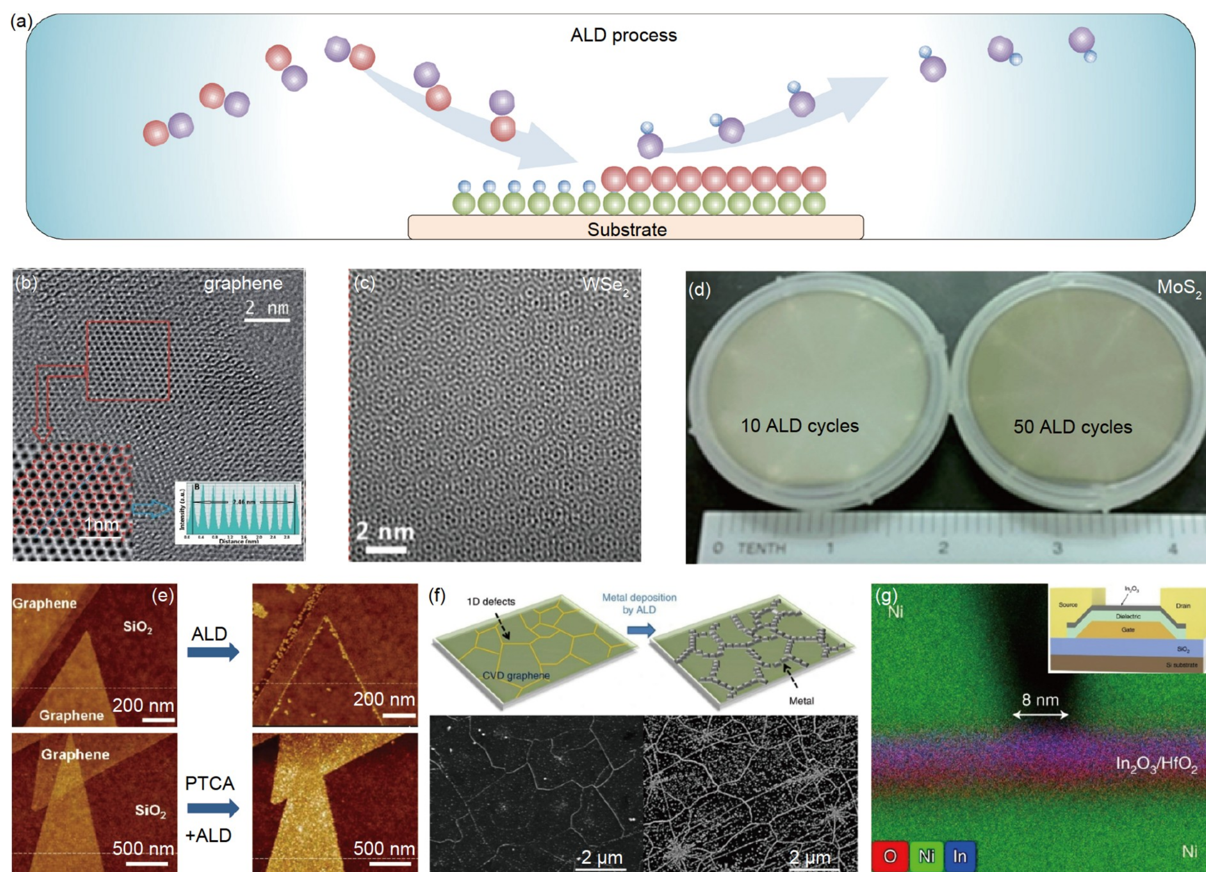

Figure 4 (Color online) Atomic layer deposition method. (a) The schematic diagram of ALD process; (b) high-resolution TEM image of the graphene; (c) high-resolution TEM image of three-layer WSe_2; (d) 10 and 50 cycles of the ALD MoS_2 film on a 2-inch sapphire (001) substrate; (e) ALD of Al_2O_3 on pristine graphene and ALD of Al_2O_3 on PTCA-coated graphene; (f) selective ALD growth on graphene; (g) high-angle annular dark-field STEM cross-sectional image with energy-dispersive X-ray spectroscopy (EDX) elemental mapping of an In_2O_3 transistor. (b) Reproduced with permission from ref. [70]. Copyright©Royal Society of Chemistry. (c) Reproduced with permission from ref. [71]. Copyright©IOP Publishing. (d) Reproduced with permission from ref. [72]. Copyright©Royal Society of Chemistry. (e) Reproduced with permission from ref. [73]. Copyright©(2008) American Chemical Society. (f), (g) Reproduced with permission from refs. [74,75], respectively. Copyright©Springer Nature.

graphene. They successfully achieved the enhanced chemical reactivity of these line defects for the application of high-performance hydrogen gas sensors (Figure 4(f)). What is more, semiconductor processing is also one of the main application fields for the recent development of ALD. Si et al. [75] reported the In_2O_3 transistors fabricated by ALD. The channel lengths could be down to 8.0 nm and channel thicknesses down could be to 0.50 nm. The equivalent dielectric oxide thickness is down to 0.84 nm (Figure 4(g)).

ALD has recently been investigated as a new technique for synthesizing 2D quantum materials due to its atomic-level precision, thin-film uniformity, conformality on substrates of any shape, and the advantages of growth at low temperatures even down to room temperature. About 25 types of 2D quantum materials and over 80 ALD processes have been reported in the past decades [83]. With the development of the ALD process, researchers can produce large-scale high-quality 2D quantum materials more precisely.

5 Physical vapor deposition method (PVD)

PVD is a vacuum deposition method to produce high-quality solid materials in a physical way. The common PVD processes are sputtering and evaporation. PVD is developed in the 1850s due to the evolution of vacuum electric technology in the mid-1600s [84]. The first documented evaporation experiment was carried out in the early 1870s by Stefan and in the early 1880s by Hertz [85]. At the 1960 Electrochemical Society meeting in Houston, TX, Blocher, from Battelle Columbus (OH) Laboratory coined the term “PVD” [85]. In 1966, Powell et al. [86] pointed out the physical vapor deposition technique in a book entitled Vapor Deposition, which is used to distinguish it from other deposition methods.

About the process of PVD, the solid material to be deposited is converted into a gaseous state by high-temperature heating first. And then it moves to the vicinity of the substrate under the airflow. Finally, the vapor reconstructs on the substrate surface to form a thin film (Figure 5(a)). PVD is a

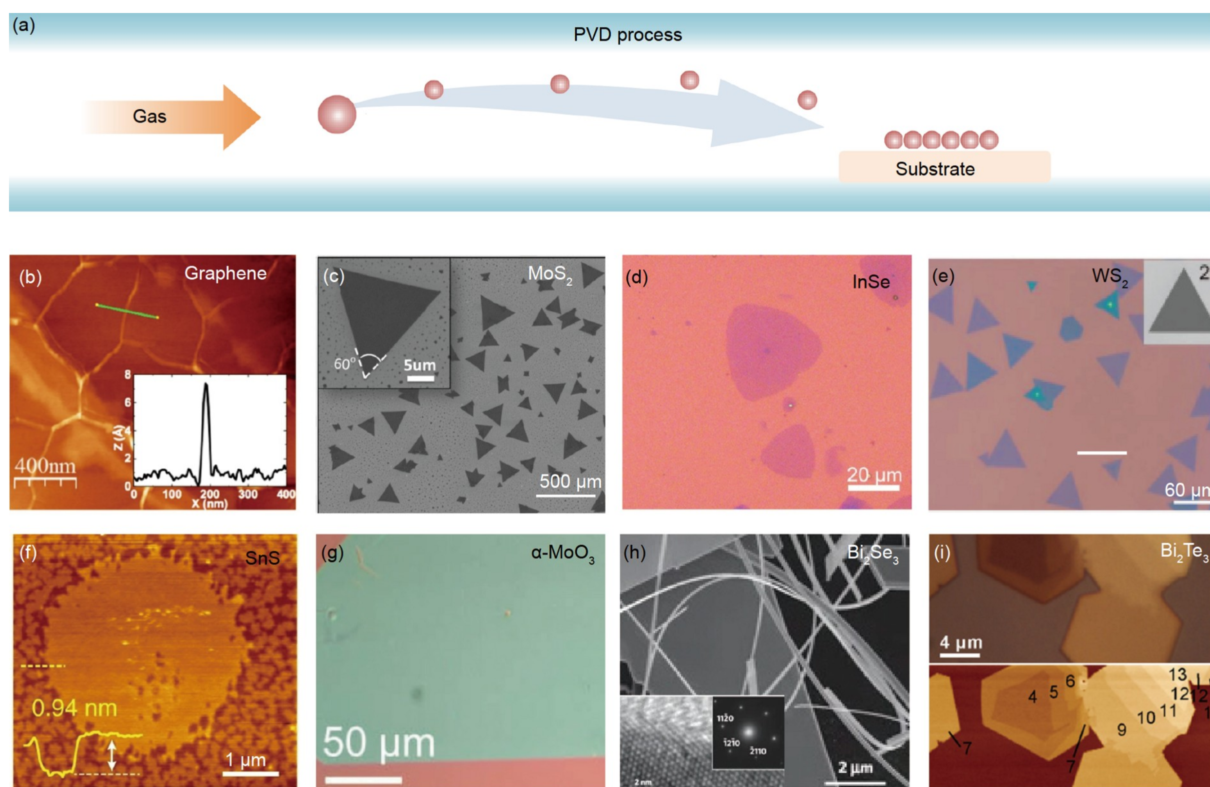

Figure 5 (Color online) Physical vapor deposition method. (a) The schematic diagram of PVD process; (b) AFM images of the graphene layer grown on the Cu foil by the decomposition of C_{60} molecules. (c) Scanning electron microscopy (SEM) image of triangular MoS_2 monolayer crystallites grown on a 300 nm SiO_2/Si substrate. The inset shows the 60 corners of a selected crystallite with a clean surface. (d) Optical image of monolayer InSe. (e) 3R phase WS_2 with different shapes in different regions. The inset shows typical SEM image of 3R phase WS_2. (f) AFM image of SnS crystals with different thicknesses from bulk to monolayer; (g) optical image of large-scale α-MoO_3 crystals; (h) SEM image of as-grown nanoribbons from Bi_2Se_3 evaporation. (i) High-magnification optical image and AFM image of Bi_2Te_3 with multiple step edges. The number of quintuple layers is marked in AFM (black). (b) Reproduced with permission from ref. [87]. Copyright©Royal Society of Chemistry. (c) Reproduced with permission of ref. [88]. Copyright©ACS Publications. (d) Reproduced with permission from ref. [89]. Copyright©IOP Publishing. (e) Reproduced with permission of ref. [90]. Copyright©John Wiley and Sons. (f) Reproduced with permission from ref. [91]. Copyright©Springer Nature. (g) Reproduced with permission of ref. [92]. Copyright©IOP Publishing. (h) Reproduced with permission from ref. [93]. Copyright©Springer Nature. (i) Reprinted (adapted) with permission from [94]. Copyright©American Chemical Society.

vaporization coating technique that involves the transfer of material at the atomic level. Coatings deposited by PVD tend to have thin thicknesses, which can range from atomic layers to several microns. At the same time, it has low environmental requirements, so it has wide application potential in the semiconductor industry.

For 2D quantum materials, PVD is also a convenient synthesis method. High-quality PVD graphene growth by fullerene decomposition on Cu foils was reported in 2017 [87] (Figure 5(b)). Wu et al. [88] synthesized high-quality monolayer MoS_2 single crystals up to 25 μm in size on a variety of standard insulating substrates (SiO_2, sapphire and glass) by PVD (Figure 5(c)). Zhou et al. [89] demonstrated the successful synthesis of monolayer InSe by PVD (Figure 5(d)). Zeng et al. [90] synthesized large-area triangular 3R phase WS_2 and WSe_2 with different layer thicknesses (Figure 5(e)).

Importantly, PVD provides convenience for the exploration of 2D quantum material properties and applications. Higashitarumizu et al. [91] explored the purely in-plane ferroelectricity in monolayer SnS synthesized by PVD (Figure 5(f)). Zhong et al. [92] reported controllable growth of large-size 2D α-MoO_3 single crystals with a few nanometers thick and over 300 μm in lateral size for high-performance solar-blind photodetectors (Figure 5(g)).

PVD is also a powerful method for the research on the topological insulator. Peng et al. [93] observed Aharonov-Bohm oscillation in Bi_2Se_3 nanoribbons, providing direct transport evidence of the robust, conducting surface states (Figure 5(h)). Kong et al. [94] reported the synthesis and characterizations of ultrathin Bi_2Te_3 and Bi_2Se_3 nanoplates with thickness down to 3 nm (3 quintuple layers) by PVD (Figure 5(i)).

PVD is a widely used technique for the fabrication of thin films and surface coatings. PVD technology has a low impact on the environment and can control the composition and thickness of the film well, which provides great convenience for the synthesis of 2D quantum materials, but the demand for raw materials limits some of its applications.

6 Chemical vapor transport method (CVT)

CVT is a synthetic method that a condensed phase (typically a solid) is volatilized in the presence of a gaseous reactant (transport agent) and deposited elsewhere usually in the form of crystals. The history of CVT can date back to the 1850s. Bunsen was the first man to describe a vapor transport reaction about the formation of hematite in nature in 1852. Many scientists including Saint-Claire-Deville, Troost, Hautefeuille, Mond and Biltz, et al., made great contributions to the early observation and experiments of the CVT technique. Werner Fischer was the first to clarify the basic principle of a CVT process in 1932. Later, Harald Schäfer described CVT qualitatively and quantitatively, and build a model, which is of great significance for the subsequent promotion and wide application of CVT [95].

A CVT process usually reacts in a closed system: in the sublimation zone (temperature T_1), the solid sources react with the transport agent to form a gaseous intermediate, which increases the pressure of the gaseous intermediate in this region, resulting in a flow to the deposition zone; in the deposition zone (temperature T_2), the gaseous intermediates are decomposed into solid sources and transport agent. The solid sources then undergo chemical reactions to generate the target crystal product, and the released transport agent increases the partial pressure here so that it can flow back to the sublimation zone for further reaction. In this way, a small amount of transport agent continuously circulates and transports solid sources in the sublimation zone and the deposition zone, and promotes the continuous synthesis of the target product [96,97] (Figure 6(a)). Using this method, large-scale single crystal samples can be finally produced.

Thousands of materials including intermetallic, halides, oxides, sulfides, selenides, tellurides, chalcogenide-halides and pnictides have been synthesized by CVT [95], which also provide the possibility for the preparation of 2D quantum materials. WTe_2 bulk crystal was produced by CVT with bromine as the transport agent [98] (Figure 6(b)). Alloy like $WSe_{2(1-x)}Te_{2x\,(x=0\text{-}1)}$ was also prepared by CVT with iodide as the transport agent [99] (Figure 6(c)). With suitable precursors, selectively doped samples can be also prepared. Li et al. [100] prepared the high-quality Fe-doped SnS_2 by CVT for field-effect transistors (Figure 6(d) and (e)).

For materials that are not stable in air, like black phosphorus (BP), CVT method is very suitable for their growth due to its sealing properties. Using CVT technology, BP with large size, good crystallinity and high yield can be obtained, and it is now widely used in the preparation of BP [101] (Figure 6(f)). Since CVT always produced crystals with high qualities, the obtained samples are commonly exfoliated into monolayers or few layers to carry out the further investigation [102] (Figure 6(g)). Besides the exfoliation of an as-grown sample, by reducing the temperature gradient, the concentration of reactants, and choosing a suitable transport agent to slow down the reaction rate, even monolayer samples can be prepared using the CVT method. Jiao's group has successfully prepared several 2D monolayer materials, including $TiSe_2$ [103] (Figure 6(h)), MoS_2 (Figure 6(i)), WS_2, $MoSe_2$, $Mo_xW_{1-x}S_2$ and ReS_2 [104].

CVT technology has unique advantages in the preparation of single-crystal bulk materials. Combined with mechanical exfoliation technology, it provides a high-quality sample for the exploration of the properties of 2D quantum materials. Currently, it is more widely used in the manufacture of TMDs and BP and it can also find its place in the preparation

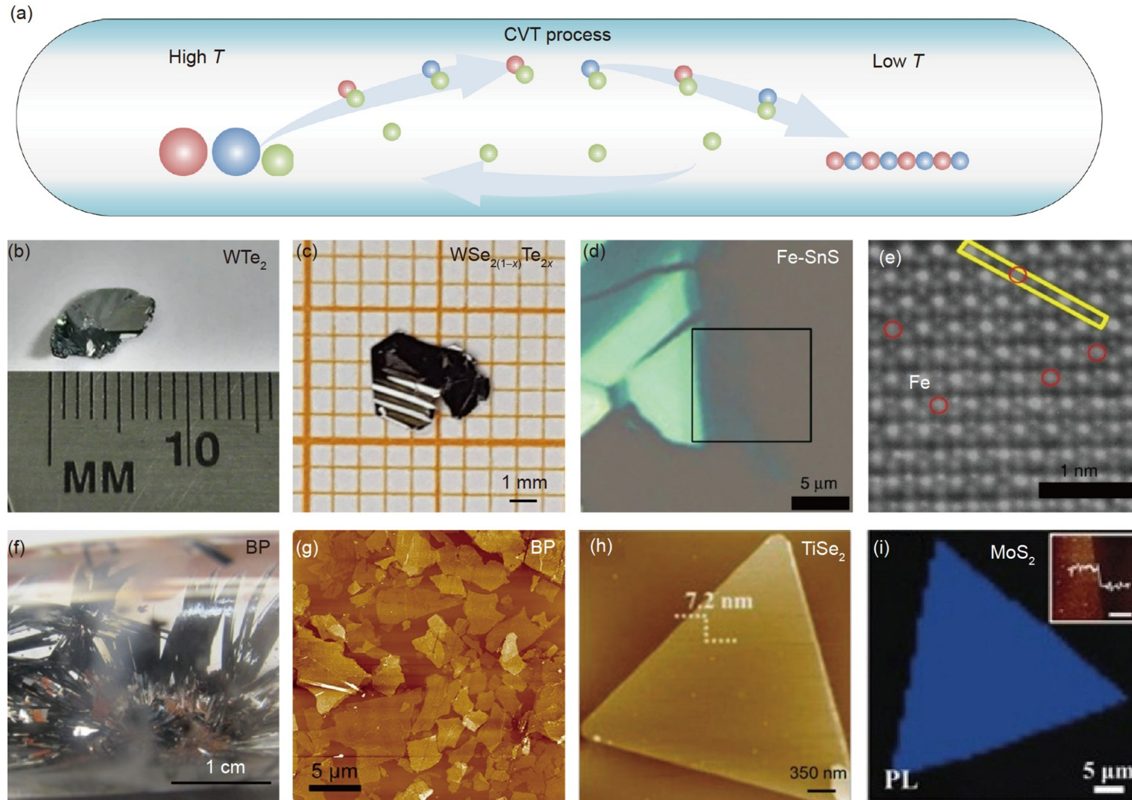

Figure 6 (Color online) Chemical vapor transport method. (a) The schematic diagram of CVT process; (b) photograph of WTe_2 large bulk crystal; (c) photograph of 2H $WSe_{1.4}Te_{0.6}$ large bulk crystal; (d) optical image of the $Fe_{0.021}Sn_{0.979}S_2$ flake. (e) High-resolution STEM image of the $Fe_{0.021}Sn_{0.979}S_2$ flake. The red circles are Fe atoms. (f) The magnified photo of BP micro ribbons; (g) AFM image of few-layer BP flakes on a SiO_2/Si substrate; (h) AFM image of thin $TiSe_2$ flakes; (i) AFM image of thin MoS_2 flake. (b) Reproduced with permission from ref. [98]. Copyright©Springer Nature. (c) Reproduced with permission from ref. [99]. Copyright©John Wiley and Sons. (d), (e) Reproduced with permission from ref. [100]. Copyright©Springer Nature. (f) Reprinted (adapted) with permission from ref. [101]. Copyright©(2016) American Chemical Society. (g) Reprinted (adapted) with permission from ref. [102]. Copyright©(2018) American Chemical Society. (h) Reprinted (adapted) with permission from ref. [103]. Copyright©(2016) American Chemical Society. (i) Reproduced with permission from ref. [104]. Copyright©John Wiley and Sons.

of other 2D quantum materials in the future.

7 Chemical vapor deposition method (CVD)

Chemical vapor deposition is a vacuum deposition method to produce high-quality and high-performance thin films in chemical ways. The earliest reported chemical synthesis of metal thin films was probably by Johann Schroeder in 1649 [85]. The production of lamp filaments and the nickel production in the 19th century promoted the development of modern CVD. Mond, van Arkel and Moers et al. have contributed a lot to CVD [105]. In 1966, the term "chemical vapor deposition" was proposed to distinguish it from other thin film growth techniques [86].

In the CVD process, the solid precursor is heated into a gaseous reactant under a specific gas atmosphere environment. The gaseous reactants are adsorbed on the heated substrate surface and then diffused. The subsequent heterogeneous chemical reactions at the gas-solid interface led to the formation of continuous thin film via nucleation, growth and coalescence. Finally, unreacted species and gaseous by-products are desorbed from the substrate surface, leaving the reactor (Figure 7(a)). In principle, there are a variety of chemical reactions and they generally have fewer requirements for vacuum environments, which broaden the application scope of CVD technology [106,107]. In the past decades, various types of CVD systems have been developed, including plasma-enhanced CVD [108] and metal-organic CVD (MOCVD) [109] techniques.

In this section, we will introduce CVD technology from three of its most famous products, i.e., graphene, h-BN and TMDs.

7.1 Graphene

As the first exfoliated 2D quantum material, graphene has led the research trend in the low-dimensional materials. The unique physical properties of graphene have great application potential in electronic and optoelectronic devices, so the preparation of large-area and high-quality graphene has long become a pursuit in material science.

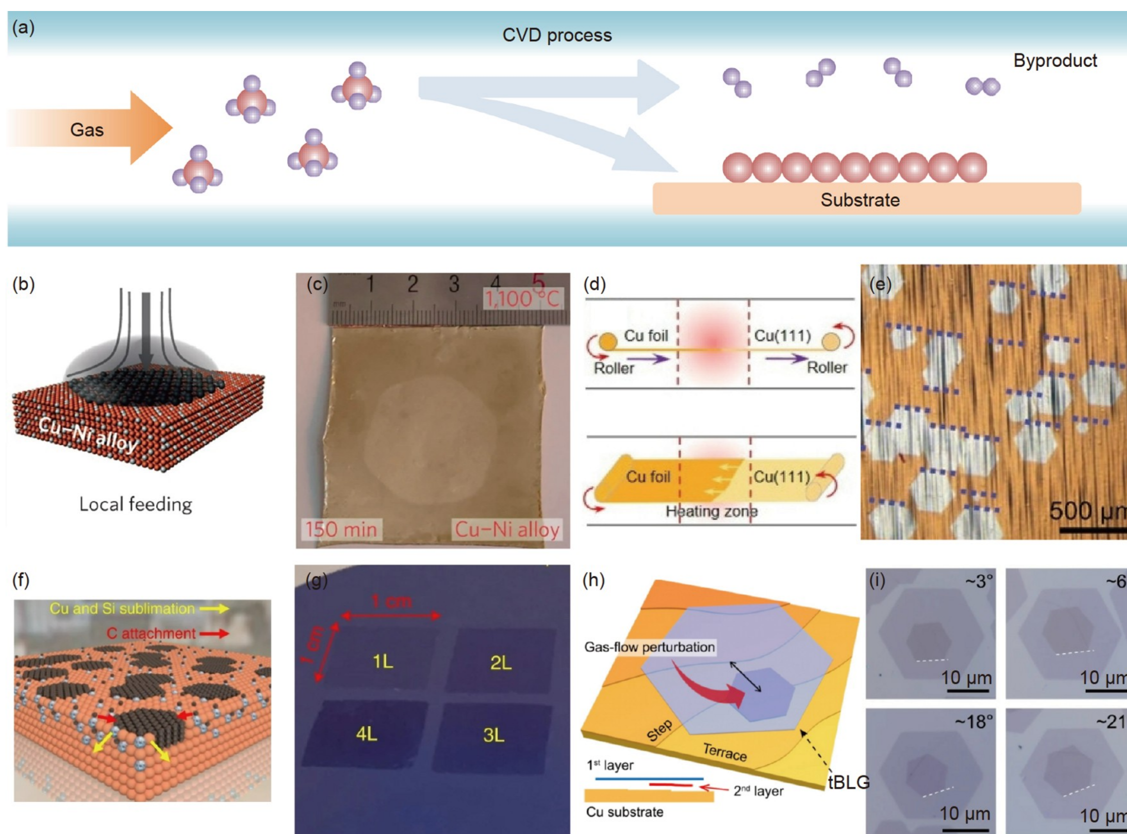

Figure 7 (Color online) Chemical vapor deposition method for graphene. (a) The schematic diagram of CVD process; (b) the schematic diagram of local feedstock feeding; (c) photograph of an ~1.5-inch single-crystal graphene on $Cu_{85}Ni_{15}$; (d) the schematic diagram of the continuous production of single-crystal Cu(111) foil; (e) optical image of unidirectionally aligned graphene domains on Cu(111); (f) the schematic diagram of diffusion-to-sublimation growth of multilayer graphene in the Cu-Si alloy; (g) photograph of centimeter-scale monolayer, bilayer, trilayer and tetralayer graphene transferred to a SiO_2/Si substrate; (h) schematic of the hetero-site nucleation for growing tBLG on a Cu substrate; (i) optical images of as-grown tBLGs with twist angles of ~3°, ~6°, ~18°, ~21°. (b), (c) Reproduced with permission from ref. [114]. Copyright©Springer Nature. (d), (e) Reproduced with permission from ref. [121]. Copyright©Elsevier. (f), (g) Reproduced with permission from ref. [127]. Copyright©Springer Nature. (h), (i) Reproduced with permission from ref. [128]. Copyright©Springer Nature.

In the past decades, a lot of research work has been devoted to improving the quality of graphene [110]. One of the methods is to suppress nucleation sites and reduce the number of polycrystalline splices, thereby reducing the density of grain boundaries. To completely eliminate the grain boundaries in solid polycrystalline Cu, Geng et al. [111] employed a liquid Cu surface system to obtain uniform nucleation distribution and low graphene nucleation density. The self-assembly of graphene flakes could be enabled into compact and ordered structures. In 2013, Zhou et al. [112] maintained a catalytic inactive Cu_2O layer during the initial nucleation stage to reduce the graphene nucleation density. Hao et al. [113] also discovered that the graphene nucleation could be decreased by oxygen on the Cu surface, and they realized the repeatable growth of centimeter-scale single-crystal graphene domains.

Another approach is increasing the single-domain growth rate and reducing the number of nucleation sites at the same time. In 2016, Wu et al. [114] designed a locally feeding carbon precursor to a desired position of an optimized Cu-Ni alloy (Figure 7(b)) and synthesized an ~1.5-inch-large graphene monolayer in 2.5 h (Figure 7(c)). A single nucleus on the entire substrate could be formatted by the localized feeding method, and an isothermal segregation mechanism was activated that greatly expedites the growth rate. Later, scientists also found that the way of specific local element supply can speed up the decomposition of reactants, which could also increase the growth rate. Xu et al. [115] and Liu et al. [116] utilize the supply of local oxygen and local fluorine, respectively, to significantly reduce the decomposition barrier of the carbon source, and even convert the endothermic reaction into an exothermic reaction. The method greatly increased the reaction rate, up to ~200 μm/s, which is the fastest growth record of graphene reported so far.

For the growth of 2D quantum materials, the method of single-domain control can only achieve the preparation of materials on the micrometer to centimeter scale. To achieve large-scale applications, it is necessary to control the coordinated growth of multiple crystal domains into one large single crystal. In 2014, Lee et al. [117] found the unidirectional alignment of multiple seeds on the germanium (110) surface due to the anisotropic twofold symmetry. It was

merged to uniform single-crystal graphene with predefined orientation. Therefore, the selection and preparation of the single-crystal substrate become the key to the growth of large-scale graphene. In theory, the size of the single-crystal substrate directly determines the epitaxial size of graphene. The surface of single-crystal Cu(111) is considered to be the most ideal substrate for the epitaxial growth of monolayer single-crystal graphene, because both the Cu(111) lattice and the graphene lattice have C3 symmetry, and the lattice mismatch degree is only 4%. Meanwhile, the epitaxial growth of graphene on Cu shows self-limiting properties [118]. Nguyen et al. [119] prepared the ultra-flat single-crystal Cu (111) film on a 2-inch sapphire by magnetron sputter using a single-crystal Cu target to grow wafer-scale single-crystal graphene. They also prepared large-area Cu(111) foil from Cu foil [120]. In 2017, Xu et al. [121] invented a method for the rapid growth of a single nucleus driven by an interface temperature gradient (Figure 7(d)) to obtain a Cu(111) single crystal. Based on that, they prepared a half-meter long single-crystal graphene film (Figure 7(e)) with >99% ultra-highly oriented grains.

For graphene, multilayer structure and its stacking order provide the fundamentally interesting properties of tuning a material from metallic to semiconductor [122,123] and even superconductor [124,125]. Huang et al. [126] reported large-area, high-quality AB-stacked bilayer and ABA-stacked trilayer graphene films on single-crystal Cu/Ni(111) alloy foils. Nguyen et al. [127] proposed an approach for controlling the layer thickness and crystallographic stacking sequence of multilayer graphene films at the wafer-scale via Cu-Si alloy (Figure 7(f) [114,121,127,128]). They reached the growth of one to four graphene layers (Figure 7(g)).

Besides the thickness control, the interlayer twist angle is another important parameter to study the physical properties of graphene [129,130], so the preparation of high-quality large-area bilayer graphene with rich rotation angles is important. Sun et al. [128] demonstrated a CVD approach for growing high-quality twisted bilayer graphene (tBLG) using a hetero-site nucleation strategy, which enables the nucleation of the second layer at a different site from that of the first layer (Figure 7(h)). They found that the fraction of tBLGs in bilayer graphene domains with twist angles ranging from 0° to 30° has been improved to 88% (Figure 7(i)).

7.2 Hexagonal boron nitride (h-BN)

h-BN, also called white graphite, is an insulating 2D quantum material [131]. It is widely used as the ideal substrate and plays an important role in the fundamental science and technology fields [132,133]. There are many recent reports on the synthesis of h-BN, among which, CVD is the most powerful way to produce large-area high-quality h-BN films.

Different from the centrosymmetric structure of graphene, the boron and nitride atoms in the h-BN lattice are alternately arranged and have a non-centrosymmetric structure. When h-BN is epitaxially grown on a centrosymmetric surface, such as Cu(111), the nucleation and growth energies of h-BN in the two orientations of 0° and 180° are degenerated, so they appear on the substrate with the same probability. With the continuous growth of the crystal domains, the two orientations of h-BN are spliced with each other to form twin grain boundaries [134]. To solve that, many efforts have been made.

In 2016, Li et al. [135] found that h-BN domains grown on onefold symmetric Cu(102) or (103) share a unique orientation. In 2019, Wang et al. [136] found that the coupling of Cu⟨211⟩ step edges with h-BN zigzag edges breaks the equivalence of antiparallel h-BN domains (Figure 8(a) [136-139]), and they realized the unidirectional single-crystal h-BN growth on Cu(110) facet (Figure 8(b)). In 2019, Chen et al. [140] constructed steps on the Cu(111) substrate, also realizing the single orientation growth of h-BN on the steps. Unlike the coupling effect between the solid substrate surface and the h-BN, h-BN also can form circular grains with interaction with liquid metals. Lee et al. [137] synthesized a single-crystal h-BN film on a liquid Au, because the limited solubility of boron and nitrogen atoms in liquid Au promotes the high diffusion of adatoms on the surface, and then provokes the circular formation of h-BN grains (Figure 8(c)). They further evolve into closely packed unimodal grains through self-collimation of boron and nitrogen edges inherited by electrostatic interaction between grains (Figure 8(d)). Similar phenomena of single-crystal self-alignment were reported on liquid Cu [141].

Compared with monolayer h-BN, the multilayer structure is also highly desired for the applications of electronic devices [142,143]. Kim et al. [138] used Fe foil (Figure 8(e)) to synthesize large-area multilayer h-BN film by CVD with a borazine precursor. Using a slow-cooling rate control, the boron and nitrogen atoms would diffuse out of the Fe surface to form multilayer h-BN (Figure 8(f)). Besides, Shi et al. [139] also reported a vapor-liquid-solid growth method to achieve uniform thick h-BN films by using molten $Fe_{82}B_{18}$ alloy and N_2 as reactants (Figure 8(g)). They finally obtained a uniform multilayer h-BN film with a thickness of 5-50 nm (Figure 8(h)).

7.3 Transition metal dichalcogenides (TMDs)

TMDs are critically important for a variety of high-end applications due to their excellent electronic and optical properties [144-146]. CVD method is also the most powerful strategy to synthesize TMD materials.

In 2012, Lee et al. [147] synthesized large-area MoS_2 atomic layers on SiO_2 by using MoO_3 and S powders as the reactants. Gao et al. [148] reported the ultrafast growth of

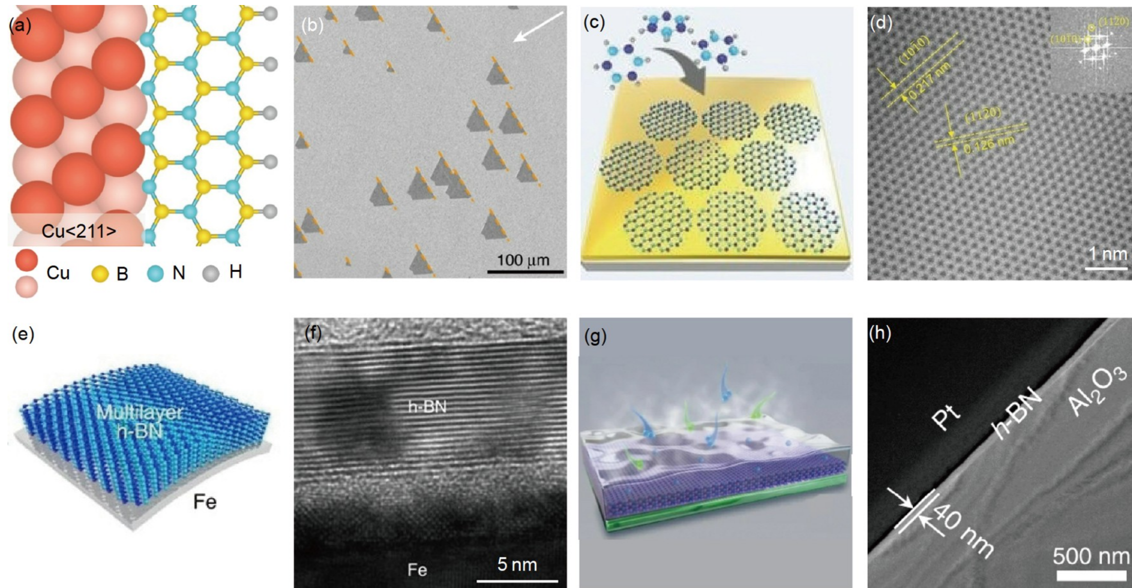

Figure 8 (Color online) Chemical vapor deposition method for h-BN. (a) The schematic diagram of the configuration of the h-BN lattice and the atomic step on Cu(110); (b) SEM image of as-grown unidirectionally aligned h-BN domains on the Cu(110) substrate; (c) the schematic diagram for the growth of single-crystalline h-BN film by means of self-collimated circular h-BN grains with a rotation invoked by the attractive Coulomb interaction of B and N edges between grains. (d) High-resolution TEM image of single-crystalline h-BN film. The inset shows the fast Fourier transform of the whole image. (e) Schematic diagram of a multilayer h-BN film frown on a Fe foil; (f) cross-sectional TEM images of an as-grown multilayer h-BN film on a Fe foil; (g) schematics of multilayer h-BN grown on sapphire with $Fe_{82}B_{18}$ alloy and nitrogen as reactants; (h) cross-sectional TEM image of multilayer h-BN on sapphire. (a), (b) Reproduced with permission from ref. [136]. Copyright©Springer Nature. (c), (d) Reproduced with permission from ref. [137]. Copyright©2018, The American Association for the Advancement of Science. (e), (f) Reproduced with permission from ref. [138]. Copyright©Springer Nature. (g), (h) Reproduced with permission from ref. [139]. Copyright©Springer Nature.

high-quality uniform monolayer WSe_2 with a growth rate of ≈26 μm s^{-1} on reusable Au substrate, which is about 2-3 orders of magnitude faster than those of most 2D TMDs grown on nonmetal substrates.

Now, using raw materials such as metal oxides and sulfur powder as precursors is the mainstream way to synthesize TMDs, but due to the high melting points of their metal and metal oxide precursors, many TMDs are difficult to produce. In 2018, Zhou et al. [149] demonstrated that molten-salt-assisted CVD method can be broadly applied for the synthesis of a wide variety of 2D TMDs. The salt decreases the melting point of the reactants and facilitates the formation of intermediate products, thus increasing the overall reaction rate (Figure 9(a) [149-153]). They successfully synthesized 47 compounds, including 32 binary compounds, 13 alloys and two heterostructure compounds. Besides, the quality of the TMDs is also an important aspect of its controllable growth. Zuo et al. [154] reported a strategy of using active chalcogen monomer supply to grow high-quality TMDs in a robust and controllable manner. They produced MoS_2 monolayers with photoluminescent circular helicity of ~92% and electronic mobility of ~42 cm^2 V^{-1} s^{-1} and a uniform quaternary TMDs alloy with three different anions. For concrete applications, the controllable synthesis of large-area monolayer TMDs is highly desired. Yang et al. [150] designed a face-to-face metal-precursor supply route (Figure 9(b)) to synthesize 6-inch uniform monolayer MoS_2 on the solid soda-lime glass. Yu et al. [151] employed independent carrier gas pathways in a three-temperature furnace to grow wafer-scale MoS_2 on single-crystal sapphire wafers (Figure 9(c)).

The direct growth of 2D quantum materials on insulating substrates is the key to advancing their future electronic device applications. However, for a long time, the epitaxial growth of TMDs on insulating substrates could not eliminate the antiparallel domain issues [155]. In 2021, Wang et al. [152] reported the successful epitaxial growth of 2-inch single-crystal WS_2 monolayer films on vicinal *a*-plane sapphire surfaces by a dual-coupling-guided mechanism (Figure 9(d) and (e)). In the meanwhile, Li et al. [156] designed the miscut orientation towards the *A* axis (*C*/*A*) of sapphire to break the degeneracy of nucleation energy for the antiparallel MoS_2 domains. This method could lead to more than a 99% unidirectional alignment. Choi et al. [157] also reported the single-crystal growth of TMDs monolayers via the atomic smooth gold surface as a universal growth template.

Despite advances in the growth of monolayer large-area single-crystal TMDs, the controlled epitaxial growth of multilayers remains a big challenge [158]. Very recently, Liu et al. [153] engineered the atomic terrace height on *c*-plane sapphire to enable an edge-nucleation mechanism (Figure 9(f)). They finally realized the uniform nucleation (>99%) of bilayer MoS_2 on a *c*-plane sapphire (Figure 9(g)). Wang et al. [159] reported the growth of high-quality mul-

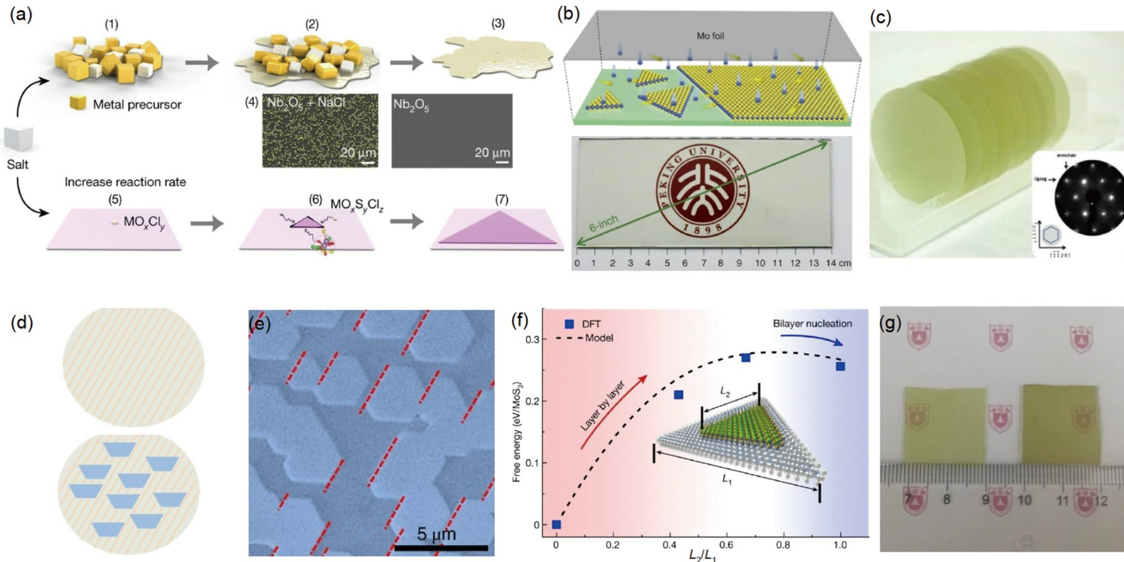

Figure 9 (Color online) Chemical vapor deposition method for TMDs. (a) The schematic diagram of the reactions of molten-salt-assisted CVD. (b) Top: schematic diagram of a face-to-face metal-precursor supply route; down: photograph of a 6-inch continuous MoS_2 film on soda-lime glass synthesized for ~8 min. (c) Photos of 2-inch MoS_2/sapphire and sapphire substrate, inset: low-energy electron diffraction (LEED) pattern; (d) schematic of the growth process of a WS_2 monolayer on vicinal *a*-plane sapphire; (e) false-color SEM image of O_2-etched WS_2 films; (f) thermodynamic analysis on different layer MoS_2 growth on *c*-plane sapphire; (g) photograph of monolayer (left) and bilayer (right) MoS_2 films on annealed sapphire substrates. (a) Reproduced with permission from ref. [149]. Copyright©Springer Nature. (b) Reproduced with permission from ref. [150]. Copyright©Springer Nature. (c) Reproduced with permission from ref. [151]. Copyright©American Chemical Society. (d), (e) Reproduced with permission from ref. [152]. Copyright©Springer Nature. (f), (g) Reproduced with permission from ref. [153]. Copyright©Springer Nature.

tilayer MoS_2 4-inch wafers via the layer-by-layer epitaxy process.

8 Summary and outlook

To summarize, the controllable preparation of 2D quantum materials is vital for manufacturing high-performance electronic and optoelectronic devices. Several preparation technologies have a profound history and demonstrate their specific advantages. In this review, we systematically summarize the synthesis methods for the controllable growth of various 2D quantum materials.

At present, the growth of single-crystal graphene and h-BN has already reached the meter or submeter scale, which meets the requirement for industrial mass production. However, the growth of other single-crystal 2D quantum materials remains at the centimeter or millimeter scale, which restricts their applications. We believe that the abovementioned technologies and strategies can help realize the preparation of various large-scale single-crystal 2D quantum materials soon.

In addition to the size, the thickness of the 2D film is an important aspect. Thicker films can integrate the properties of monolayers and demonstrate new properties beyond those of monolayers. Recently, progress has been made on the controllable growth of few-layer graphene, h-BN, and MoS_2, but the number of layers is still less than ten. A large thick single-crystal film is yet to be developed for future applications.

Furthermore, multilayer 2D quantum materials with controllable doping density, designed stacking structures, twisted angles, or specific heterostructures demonstrate considerable potential for innovation in scientific research. However, their controllable growth remains a great challenge that deserves more exploration in the future.

It is believed that the development of quantum technology is based on the quantum materials, and using the technologies summarized herein, the properties of the 2D quantum materials can be more precisely regulated to meet the needs of the various applications, thereby driving remarkable progress in today's technology.

This work was supported by the Guangdong Major Project of Basic and Applied Basic Research (Grant No. 2021B0301030002), the National Key R&D Program of China (Grant No. 2021YFA1400502), and the National Natural Science Foundation of China (Grant Nos. 52025023, and 92163206).

1 A. K. Geim, and K. S. Novoselov, Nat. Mater. **6**, 183 (2007).
2 K. S. Novoselov, V. I. Fal'ko, L. Colombo, P. R. Gellert, M. G. Schwab, and K. Kim, Nature **490**, 192 (2012).
3 S. B. Desai, S. R. Madhvapathy, A. B. Sachid, J. P. Llinas, Q. Wang, G. H. Ahn, G. Pitner, M. J. Kim, J. Bokor, C. Hu, H. S. P. Wong, and A. Javey, Science **354**, 99 (2016).
4 K. Kang, S. Xie, L. Huang, Y. Han, P. Y. Huang, K. F. Mak, C. J. Kim, D. Muller, and J. Park, Nature **520**, 656 (2015).
5 K. S. Novoselov, A. Mishchenko, A. Carvalho, and A. H. Castro Neto, Science **353**, aac9439 (2016).
6 S. Ghosh, W. Bao, D. L. Nika, S. Subrina, E. P. Pokatilov, C. N. Lau, and A. A. Balandin, Nat. Mater. **9**, 555 (2010), arXiv: 1003.5247.
7 K. S. Novoselov, A. K. Geim, S. V. Morozov, D. Jiang, Y. Zhang, S. V. Dubonos, I. V. Grigorieva, and A. A. Firsov, Science **306**, 666

(2004), arXiv: cond-mat/0410550.
8 F. Wang, Y. Zhang, C. Tian, C. Girit, A. Zettl, M. Crommie, and Y. R. Shen, Science **320**, 206 (2008).
9 A. Carvalho, M. Wang, X. Zhu, A. S. Rodin, H. Su, and A. H. Castro Neto, Nat. Rev. Mater. **1**, 16061 (2016).
10 S. Manzeli, D. Ovchinnikov, D. Pasquier, O. V. Yazyev, and A. Kis, Nat. Rev. Mater. **2**, 17033 (2017).
11 K. Watanabe, T. Taniguchi, and H. Kanda, Nat. Mater. **3**, 404 (2004).
12 M. Xu, T. Liang, M. Shi, and H. Chen, Chem. Rev. **113**, 3766 (2013).
13 C. Gong, L. Li, Z. Li, H. Ji, A. Stern, Y. Xia, T. Cao, W. Bao, C. Wang, Y. Wang, Z. Q. Qiu, R. J. Cava, S. G. Louie, J. Xia, and X. Zhang, Nature **546**, 265 (2017), arXiv: 1703.05753.
14 Y. Deng, Y. Yu, Y. Song, J. Zhang, N. Z. Wang, Z. Sun, Y. Yi, Y. Z. Wu, S. Wu, J. Zhu, J. Wang, X. H. Chen, and Y. Zhang, Nature **563**, 94 (2018), arXiv: 1803.02038.
15 S. Jiang, L. Li, Z. Wang, K. F. Mak, and J. Shan, Nat. Nanotech. **13**, 549 (2018), arXiv: 1802.07355.
16 B. Huang, G. Clark, D. R. Klein, D. MacNeill, E. Navarro-Moratalla, K. L. Seyler, N. Wilson, M. A. McGuire, D. H. Cobden, D. Xiao, W. Yao, P. Jarillo-Herrero, and X. Xu, Nat. Nanotech. **13**, 544 (2018), arXiv: 1802.06979.
17 H. Yang, J. Heo, S. Park, H. J. Song, D. H. Seo, K. E. Byun, P. Kim, I. K. Yoo, H. J. Chung, and K. Kim, Science **336**, 1140 (2012).
18 S. Goossens, G. Navickaite, C. Monasterio, S. Gupta, J. J. Piqueras, R. Pérez, G. Burwell, I. Nikitskiy, T. Lasanta, T. Galán, E. Puma, A. Centeno, A. Pesquera, A. Zurutuza, G. Konstantatos, and F. Koppens, Nat. Photon. **11**, 366 (2017), arXiv: 1701.03242.
19 L. Sun, Y. Zhang, G. Han, G. Hwang, J. Jiang, B. Joo, K. Watanabe, T. Taniguchi, Y. M. Kim, W. J. Yu, B. S. Kong, R. Zhao, and H. Yang, Nat. Commun. **10**, 3161 (2019).
20 Z. Lin, Y. Liu, U. Halim, M. Ding, Y. Liu, Y. Wang, C. Jia, P. Chen, X. Duan, C. Wang, F. Song, M. Li, C. Wan, Y. Huang, and X. Duan, Nature **562**, 254 (2018).
21 J. K. Huang, Y. Wan, J. Shi, J. Zhang, Z. Wang, W. Wang, N. Yang, Y. Liu, C. H. Lin, X. Guan, L. Hu, Z. L. Yang, B. C. Huang, Y. P. Chiu, J. Yang, V. Tung, D. Wang, K. Kalantar-Zadeh, T. Wu, X. Zu, L. Qiao, L. J. Li, and S. Li, Nature **605**, 262 (2022).
22 H. Kim, S. Z. Uddin, D. H. Lien, M. Yeh, N. S. Azar, S. Balendhran, T. Kim, N. Gupta, Y. Rho, C. P. Grigoropoulos, K. B. Crozier, and A. Javey, Nature **596**, 232 (2021).
23 C. Qin, A. S. D. Sandanayaka, C. Zhao, T. Matsushima, D. Zhang, T. Fujihara, and C. Adachi, Nature **585**, 53 (2020).
24 Y. Jiang, Z. Chen, Y. Han, P. Deb, H. Gao, S. Xie, P. Purohit, M. W. Tate, J. Park, S. M. Gruner, V. Elser, and D. A. Muller, Nature **559**, 343 (2018), arXiv: 1801.04630.
25 N. P. Wilson, W. Yao, J. Shan, and X. Xu, Nature **599**, 383 (2021).
26 A. Gao, Y. F. Liu, C. Hu, J. X. Qiu, C. Tzschaschel, B. Ghosh, S. C. Ho, D. Bérubé, R. Chen, H. Sun, Z. Zhang, X. Y. Zhang, Y. X. Wang, N. Wang, Z. Huang, C. Felser, A. Agarwal, T. Ding, H. J. Tien, A. Akey, J. Gardener, B. Singh, K. Watanabe, T. Taniguchi, K. S. Burch, D. C. Bell, B. B. Zhou, W. Gao, H. Z. Lu, A. Bansil, H. Lin, T. R. Chang, L. Fu, Q. Ma, N. Ni, and S. Y. Xu, Nature **595**, 521 (2021), arXiv: 2107.10233.
27 B. A. Bernevig, C. Felser, and H. Beidenkopf, Nature **603**, 41 (2022), arXiv: 2203.02890.
28 Y. Wu, Z. Jiang, X. Lu, Y. Liang, and H. Wang, Nature **575**, 639 (2019).
29 C. Liu, L. Wang, J. Qi, and K. Liu, Adv. Mater. **32**, 2000046 (2020).
30 M. Yi, and Z. Shen, J. Mater. Chem. A **3**, 11700 (2015).
31 M. Cai, D. Thorpe, D. H. Adamson, and H. C. Schniepp, J. Mater. Chem. **22**, 24992 (2012).
32 Y. Hernandez, V. Nicolosi, M. Lotya, F. M. Blighe, Z. Sun, S. De, I. T. McGovern, B. Holland, M. Byrne, Y. K. Gun'Ko, J. J. Boland, P. Niraj, G. Duesberg, S. Krishnamurthy, R. Goodhue, J. Hutchison, V. Scardaci, A. C. Ferrari, and J. N. Coleman, Nat. Nanotech. **3**, 563 (2008), arXiv: 0805.2850.
33 W. Zhao, M. Fang, F. Wu, H. Wu, L. Wang, and G. Chen, J. Mater. Chem. **20**, 5817 (2010).
34 C. Knieke, A. Berger, M. Voigt, R. N. K. Taylor, J. Röhrl, and W. Peukert, Carbon **48**, 3196 (2010).
35 Y. Lv, L. Yu, C. Jiang, S. Chen, and Z. Nie, RSC Adv. **4**, 13350 (2014).
36 T. Lin, Y. Tang, Y. Wang, H. Bi, Z. Liu, F. Huang, X. Xie, and M. Jiang, Energy Environ. Sci. **6**, 1283 (2013).
37 X. Y. Huang, H. Xu, C. Hui, W. Xu, L. W. Liu, J. Wei, Y. L. Wang, and H. Yuan, Acta Phys. Sin. **71**, 108201 (2022).
38 H. Xu, L. Meng, Y. Li, T. Z. Yang, L. H. Bao, G. D. Liu, L. Zhao, T. S. Liu, J. Xing, H. J. Gao, X. J. Zhou, and Y. Huang, Acta Phys. Sin. **67**, 218201 (2018).
39 G. Z. Magda, J. Pető, G. Dobrik, C. Hwang, L. P. Biró, and L. Tapasztó, Sci. Rep. **5**, 14714 (2015).
40 S. B. Desai, S. R. Madhvapathy, M. Amani, D. Kiriya, M. Hettick, M. Tosun, Y. Zhou, M. Dubey, J. W. Ager Iii, D. Chrzan, and A. Javey, Adv. Mater. **28**, 4053 (2016).
41 Y. Huang, Y. H. Pan, R. Yang, L. H. Bao, L. Meng, H. L. Luo, Y. Q. Cai, G. D. Liu, W. J. Zhao, Z. Zhou, L. M. Wu, Z. L. Zhu, M. Huang, L. W. Liu, L. Liu, P. Cheng, K. H. Wu, S. B. Tian, C. Z. Gu, Y. G. Shi, Y. F. Guo, Z. G. Cheng, J. P. Hu, L. Zhao, G. H. Yang, E. Sutter, P. Sutter, Y. L. Wang, W. Ji, X. J. Zhou, and H. J. Gao, Nat. Commun. **11**, 2453 (2020), arXiv: 2002.05025.
42 M. Velický, G. E. Donnelly, W. R. Hendren, S. McFarland, D. Scullion, W. J. I. DeBenedetti, G. C. Correa, Y. Han, A. J. Wain, M. A. Hines, D. A. Muller, K. S. Novoselov, H. D. Abruña, R. M. Bowman, E. J. G. Santos, and F. Huang, ACS Nano **12**, 10463 (2018).
43 M. Heyl, D. Burmeister, T. Schultz, S. Pallasch, G. Ligorio, N. Koch, and E. J. W. List-Kratochvil, Phys. Status Solidi RRL **14**, 2000408 (2020).
44 J. Shim, S. H. Bae, W. Kong, D. Lee, K. Qiao, D. Nezich, Y. J. Park, R. Zhao, S. Sundaram, X. Li, H. Yeon, C. Choi, H. Kum, R. Yue, G. Zhou, Y. Ou, K. Lee, J. Moodera, X. Zhao, J. H. Ahn, C. Hinkle, A. Ougazzaden, and J. Kim, Science **362**, 665 (2018).
45 J. Y. Moon, M. Kim, S. I. Kim, S. Xu, J. H. Choi, D. Whang, K. Watanabe, T. Taniguchi, D. S. Park, J. Seo, S. H. Cho, S. K. Son, and J. H. Lee, Sci. Adv. **6**, eabc6601 (2020).
46 F. Liu, W. Wu, Y. Bai, S. H. Chae, Q. Li, J. Wang, J. Hone, and X. Y. Zhu, Science **367**, 903 (2020).
47 Z. Huang, A. Alharbi, W. Mayer, E. Cuniberto, T. Taniguchi, K. Watanabe, J. Shabani, and D. Shahrjerdi, Nat. Commun. **11**, 3029 (2020).
48 K. S. Novoselov, A. K. Geim, S. V. Morozov, D. Jiang, M. I. Katsnelson, I. V. Grigorieva, S. V. Dubonos, and A. A. Firsov, Nature **438**, 197 (2005), arXiv: cond-mat/0509330.
49 Y. Zhang, Y. W. Tan, H. L. Stormer, and P. Kim, Nature **438**, 201 (2005), arXiv: cond-mat/0509355.
50 A. Y. Cho, and J. R. Arthur, Prog. Solid State Chem. **10**, 157 (1975).
51 J. R. Arthur Jr., J. Appl. Phys. **39**, 4032 (1968).
52 W. Nunn, T. K. Truttmann, and B. Jalan, J. Mater. Res. **36**, 4846 (2021).
53 W. P. McCray, Nat. Nanotech. **2**, 259 (2007).
54 L. Meng, Y. Wang, L. Zhang, S. Du, R. Wu, L. Li, Y. Zhang, G. Li, H. Zhou, W. A. Hofer, and H. J. Gao, Nano Lett. **13**, 685 (2013).
55 B. Feng, J. Zhang, Q. Zhong, W. Li, S. Li, H. Li, P. Cheng, S. Meng, L. Chen, and K. Wu, Nat. Chem. **8**, 563 (2016), arXiv: 1512.05029.
56 F. F. Zhu, W. J. Chen, Y. Xu, C. L. Gao, D. D. Guan, C. H. Liu, D. Qian, S. C. Zhang, and J. F. Jia, Nat. Mater. **14**, 1020 (2015), arXiv: 1506.01601.
57 D. Ji, S. Cai, T. R. Paudel, H. Sun, C. Zhang, L. Han, Y. Wei, Y. Zang, M. Gu, Y. Zhang, W. Gao, H. Huyan, W. Guo, D. Wu, Z. Gu, E. Y. Tsymbal, P. Wang, Y. Nie, and X. Pan, Nature **570**, 87 (2019).
58 M. M. Ugeda, A. J. Bradley, Y. Zhang, S. Onishi, Y. Chen, W. Ruan, C. Ojeda-Aristizabal, H. Ryu, M. T. Edmonds, H. Z. Tsai, A. Riss, S. K. Mo, D. Lee, A. Zettl, Z. Hussain, Z. X. Shen, and M. F. Crommie, Nat. Phys. **12**, 92 (2016), arXiv: 1506.08460.

59 Y. Zhang, K. He, Y. Zhang, K. He, C. Z. Chang, C. L. Song, L. L. Wang, X. Chen, J. F. Jia, Z. Fang, X. Dai, W. Y. Shan, S. Q. Shen, Q. Niu, X. L. Qi, S. C. Zhang, X. C. Ma, and Q. K. Xue, Nat. Phys. **6**, 584 (2010).
60 X. Zhao, P. Song, C. Wang, A. C. Riis-Jensen, W. Fu, Y. Deng, D. Wan, L. Kang, S. Ning, J. Dan, T. Venkatesan, Z. Liu, W. Zhou, K. S. Thygesen, X. Luo, S. J. Pennycook, and K. P. Loh, Nature **581**, 171 (2020).
61 S. Kezilebieke, M. N. Huda, V. Vaňo, M. Aapro, S. C. Ganguli, O. J. Silveira, S. Głodzik, A. S. Foster, T. Ojanen, and P. Liljeroth, Nature **588**, 424 (2020), arXiv: 2002.02141.
62 V. Vaňo, M. Amini, S. C. Ganguli, G. Chen, J. L. Lado, S. Kezilebieke, and P. Liljeroth, Nature **599**, 582 (2021).
63 R. Yan, G. Khalsa, S. Vishwanath, Y. Han, J. Wright, S. Rouvimov, D. S. Katzer, N. Nepal, B. P. Downey, D. A. Muller, H. G. Xing, D. J. Meyer, and D. Jena, Nature **555**, 183 (2018).
64 D. C. Tsui, H. L. Stormer, and A. C. Gossard, Phys. Rev. Lett. **48**, 1559 (1982).
65 M. Konig, S. Wiedmann, C. Brune, A. Roth, H. Buhmann, L. W. Molenkamp, X. L. Qi, and S. C. Zhang, Science **318**, 766 (2007), arXiv: 0710.0582.
66 C. Z. Chang, J. Zhang, X. Feng, J. Shen, Z. Zhang, M. Guo, K. Li, Y. Ou, P. Wei, L. L. Wang, Z. Q. Ji, Y. Feng, S. Ji, X. Chen, J. Jia, X. Dai, Z. Fang, S. C. Zhang, K. He, Y. Wang, L. Lu, X. C. Ma, and Q. K. Xue, Science **340**, 167 (2013), arXiv: 1605.08829.
67 L. Niinistö, and M. Leskelä, Thin Solid Films **225**, 130 (1993).
68 S. M. George, Chem. Rev. **110**, 111 (2010).
69 M. Ahonen, M. Pessa, and T. Suntola, Thin Solid Films **65**, 301 (1980).
70 Y. Zhang, W. Ren, Z. Jiang, S. Yang, W. Jing, P. Shi, X. Wu, and Z. G. Ye, J. Mater. Chem. C **2**, 7570 (2014).
71 K. Park, Y. Kim, J. G. Song, S. J. Kim, C. W. Lee, G. H. Ryu, Z. Lee, J. Park, and H. Kim, 2D Mater. **3**, 014004 (2016).
72 L. K. Tan, B. Liu, J. H. Teng, S. Guo, H. Y. Low, H. R. Tan, C. Y. T. Chong, R. B. Yang, and K. P. Loh, Nanoscale **6**, 10584 (2014).
73 X. Wang, S. M. Tabakman, and H. Dai, J. Am. Chem. Soc. **130**, 8152 (2008).
74 K. Kim, H. B. R. Lee, R. W. Johnson, J. T. Tanskanen, N. Liu, M. G. Kim, C. Pang, C. Ahn, S. F. Bent, and Z. Bao, Nat. Commun. **5**, 4781 (2014), arXiv: 1410.5153.
75 M. Si, Z. Lin, Z. Chen, X. Sun, H. Wang, and P. D. Ye, Nat. Electron. **5**, 164 (2022).
76 P. O. Oviroh, R. Akbarzadeh, D. Pan, R. A. M. Coetzee, and T. C. Jen, Sci. Tech. Adv. Mater. **20**, 465 (2019).
77 R. L. Puurunen, J. Appl. Phys. **97**, 121301 (2005).
78 C. Bjelkevig, Z. Mi, J. Xiao, P. A. Dowben, L. Wang, W. N. Mei, and J. A. Kelber, J. Phys.-Condens. Matter. **22**, 302002 (2010).
79 H. Park, T. K. Kim, S. W. Cho, H. S. Jang, S. I. Lee, and S. Y. Choi, Sci. Rep. **7**, 40091 (2017).
80 T. J. Dai, X. D. Fan, Y. X. Ren, S. Hou, Y. Y. Zhang, L. X. Qian, Y. R. Li, and X. Z. Liu, J. Mater. Sci. **53**, 8436 (2018).
81 B. Groven, A. Nalin Mehta, H. Bender, J. Meersschaut, T. Nuytten, P. Verdonck, T. Conard, Q. Smets, T. Schram, B. Schoenaers, A. Stesmans, V. Afanas'ev, W. Vandervorst, M. Heyns, M. Caymax, I. Radu, and A. Delabie, Chem. Mater. **30**, 7648 (2018).
82 P. Sinsermsuksakul, J. Heo, W. Noh, A. S. Hock, and R. G. Gordon, Adv. Energy Mater. **1**, 1116 (2011).
83 J. Cai, X. Han, X. Wang, and X. Meng, Matter **2**, 587 (2020).
84 J. E. Greene, Appl. Phys. Rev. **1**, 041302 (2014).
85 J. E. Greene, J. Vacuum Sci. Tech. A-Vacuum Surf. Films **35**, 05C204 (2017).
86 J. H. O. C. F. Powell, J. M. Blocher Jr., and J. Klerer, *Vapor Deposition* (Academic, New York, 1966).
87 J. Azpeitia, G. Otero-Irurueta, I. Palacio, J. I. Martinez, N. Ruiz del Árbol, G. Santoro, A. Gutiérrez, L. Aballe, M. Foerster, M. Kalbac, V. Vales, F. J. Mompeán, M. García-Hernández, J. A. Martín-Gago, C. Munuera, and M. F. López, Carbon **119**, 535 (2017).
88 S. Wu, C. Huang, G. Aivazian, J. S. Ross, D. H. Cobden, and X. Xu, ACS Nano **7**, 2768 (2013).
89 J. Zhou, J. Shi, Q. Zeng, Y. Chen, L. Niu, F. Liu, T. Yu, K. Suenaga, X. Liu, J. Lin, and Z. Liu, 2D Mater. **5**, 025019 (2018).
90 Z. Zeng, X. Sun, D. Zhang, W. Zheng, X. Fan, M. He, T. Xu, L. Sun, X. Wang, and A. Pan, Adv. Funct. Mater. **29**, 1806874 (2019).
91 N. Higashitarumizu, H. Kawamoto, C. J. Lee, B. H. Lin, F. H. Chu, I. Yonemori, T. Nishimura, K. Wakabayashi, W. H. Chang, and K. Nagashio, Nat. Commun. **11**, 2428 (2020), arXiv: 2006.10441.
92 M. Zhong, K. Zhou, Z. Wei, Y. Li, T. Li, H. Dong, L. Jiang, J. Li, and W. Hu, 2D Mater. **5**, 035033 (2018).
93 H. Peng, K. Lai, D. Kong, S. Meister, Y. Chen, X. L. Qi, S. C. Zhang, Z. X. Shen, and Y. Cui, Nat. Mater. **9**, 225 (2010), arXiv: 0908.3314.
94 D. Kong, W. Dang, J. J. Cha, H. Li, S. Meister, H. Peng, Z. Liu, and Y. Cui, Nano Lett. **10**, 2245 (2010), arXiv: 1004.1767.
95 M. Binnewies, R. Glaum, M. Schmidt, and P. Schmidt, Z. Anorg. Allg. Chem. **639**, 219 (2013).
96 D. Wang, F. Luo, M. Lu, X. Xie, L. Huang, and W. Huang, Small **15**, 1804404 (2019).
97 M. Binnewies, R. Glaum, M. Schmidt, and P. Schmidt, *Chemical Vapor Transport Reactions* (Academic, Berlin, Boston, 2012).
98 C. H. Lee, E. C. Silva, L. Calderin, M. A. T. Nguyen, M. J. Hollander, B. Bersch, T. E. Mallouk, and J. A. Robinson, Sci. Rep. **5**, 10013 (2015).
99 P. Yu, J. Lin, L. Sun, Q. L. Le, X. Yu, G. Gao, C. H. Hsu, D. Wu, T. R. Chang, Q. Zeng, F. Liu, Q. J. Wang, H. T. Jeng, H. Lin, A. Trampert, Z. Shen, K. Suenaga, and Z. Liu, Adv. Mater. **29**, 1603991 (2017).
100 B. Li, T. Xing, M. Zhong, L. Huang, N. Lei, J. Zhang, J. Li, and Z. Wei, Nat. Commun. **8**, 1958 (2017).
101 M. Zhao, H. Qian, X. Niu, W. Wang, L. Guan, J. Sha, and Y. Wang, Cryst. Growth Des. **16**, 1096 (2016).
102 J. Li, C. Chen, S. Liu, J. Lu, W. P. Goh, H. Fang, Z. Qiu, B. Tian, Z. Chen, C. Yao, W. Liu, H. Yan, Y. Yu, D. Wang, Y. Wang, M. Lin, C. Su, and J. Lu, Chem. Mater. **30**, 2742 (2018).
103 J. Wang, H. Zheng, G. Xu, L. Sun, D. Hu, Z. Lu, L. Liu, J. Zheng, C. Tao, and L. Jiao, J. Am. Chem. Soc. **138**, 16216 (2016).
104 D. Hu, G. Xu, L. Xing, X. Yan, J. Wang, J. Zheng, Z. Lu, P. Wang, X. Pan, and L. Jiao, Angew. Chem. Int. Ed. **56**, 3611 (2017).
105 R. Haubner, Int. J. Refractory Met. Hard Mater. **41**, 22 (2013).
106 Z. Cai, B. Liu, X. Zou, and H. M. Cheng, Chem. Rev. **118**, 6091 (2018).
107 L. Lin, B. Deng, J. Sun, H. Peng, and Z. Liu, Chem. Rev. **118**, 9281 (2018).
108 D. E. Carlson, and C. R. Wronski, Appl. Phys. Lett. **28**, 671 (1976).
109 H. M. Manasevit, J. Cryst. Growth **55**, 1 (1981).
110 Y. Zhang, L. Zhang, and C. Zhou, Acc. Chem. Res. **46**, 2329 (2013).
111 D. Geng, B. Wu, Y. Guo, L. Huang, Y. Xue, J. Chen, G. Yu, L. Jiang, W. Hu, and Y. Liu, Proc. Natl. Acad. Sci. USA **109**, 7992 (2012).
112 H. Zhou, W. J. Yu, L. Liu, R. Cheng, Y. Chen, X. Huang, Y. Liu, Y. Wang, Y. Huang, and X. Duan, Nat. Commun. **4**, 2096 (2013).
113 Y. Hao, M. S. Bharathi, L. Wang, Y. Liu, H. Chen, S. Nie, X. Wang, H. Chou, C. Tan, B. Fallahazad, H. Ramanarayan, C. W. Magnuson, E. Tutuc, B. I. Yakobson, K. F. McCarty, Y. W. Zhang, P. Kim, J. Hone, L. Colombo, and R. S. Ruoff, Science **342**, 720 (2013).
114 T. Wu, X. Zhang, Q. Yuan, J. Xue, G. Lu, Z. Liu, H. Wang, H. Wang, F. Ding, Q. Yu, X. Xie, and M. Jiang, Nat. Mater. **15**, 43 (2016).
115 X. Xu, Z. Zhang, L. Qiu, J. Zhuang, L. Zhang, H. Wang, C. Liao, H. Song, R. Qiao, P. Gao, Z. Hu, L. Liao, Z. Liao, D. Yu, E. Wang, F. Ding, H. Peng, and K. Liu, Nat. Nanotech. **11**, 930 (2016).
116 C. Liu, X. Xu, L. Qiu, M. Wu, R. Qiao, L. Wang, J. Wang, J. Niu, J. Liang, X. Zhou, Z. Zhang, M. Peng, P. Gao, W. Wang, X. Bai, D. Ma, Y. Jiang, X. Wu, D. Yu, E. Wang, J. Xiong, F. Ding, and K. Liu, Nat. Chem. **11**, 730 (2019).
117 J. H. Lee, E. K. Lee, W. J. Joo, Y. Jang, B. S. Kim, J. Y. Lim, S. H. Choi, S. J. Ahn, J. R. Ahn, M. H. Park, C. W. Yang, B. L. Choi, S. W. Hwang, and D. Whang, Science **344**, 286 (2014).

118 X. Li, W. Cai, J. An, S. Kim, J. Nah, D. Yang, R. Piner, A. Velamakanni, I. Jung, E. Tutuc, S. K. Banerjee, L. Colombo, and R. S. Ruoff, Science **324**, 1312 (2009), arXiv: 0905.1712.
119 V. L. Nguyen, D. J. Perello, S. Lee, C. T. Nai, B. G. Shin, J. G. Kim, H. Y. Park, H. Y. Jeong, J. Zhao, Q. A. Vu, S. H. Lee, K. P. Loh, S. Y. Jeong, and Y. H. Lee, Adv. Mater. **28**, 8177 (2016).
120 V. L. Nguyen, B. G. Shin, D. L. Duong, S. T. Kim, D. Perello, Y. J. Lim, Q. H. Yuan, F. Ding, H. Y. Jeong, H. S. Shin, S. M. Lee, S. H. Chae, Q. A. Vu, S. H. Lee, and Y. H. Lee, Adv. Mater. **27**, 1376 (2015).
121 X. Xu, Z. Zhang, J. Dong, D. Yi, J. Niu, M. Wu, L. Lin, R. Yin, M. Li, J. Zhou, S. Wang, J. Sun, X. Duan, P. Gao, Y. Jiang, X. Wu, H. Peng, R. S. Ruoff, Z. Liu, D. Yu, E. Wang, F. Ding, and K. Liu, Sci. Bull. **62**, 1074 (2017), arXiv: 1707.02512.
122 S. Latil, and L. Henrard, Phys. Rev. Lett. **97**, 036803 (2006).
123 R. R. Nair, P. Blake, A. N. Grigorenko, K. S. Novoselov, T. J. Booth, T. Stauber, N. M. R. Peres, and A. K. Geim, Science **320**, 1308 (2008).
124 Y. Cao, V. Fatemi, S. Fang, K. Watanabe, T. Taniguchi, E. Kaxiras, and P. Jarillo-Herrero, Nature **556**, 43 (2018), arXiv: 1803.02342.
125 M. Yankowitz, S. Chen, H. Polshyn, Y. Zhang, K. Watanabe, T. Taniguchi, D. Graf, A. F. Young, and C. R. Dean, Science **363**, 1059 (2019), arXiv: 1808.07865.
126 M. Huang, P. V. Bakharev, Z. J. Wang, M. Biswal, Z. Yang, S. Jin, B. Wang, H. J. Park, Y. Li, D. Qu, Y. Kwon, X. Chen, S. H. Lee, M. G. Willinger, W. J. Yoo, Z. Lee, and R. S. Ruoff, Nat. Nanotechnol. **15**, 289 (2020).
127 V. L. Nguyen, D. L. Duong, S. H. Lee, J. Avila, G. Han, Y. M. Kim, M. C. Asensio, S. Y. Jeong, and Y. H. Lee, Nat. Nanotechnol. **15**, 861 (2020).
128 L. Sun, Z. Wang, Y. Wang, L. Zhao, Y. Li, B. Chen, S. Huang, S. Zhang, W. Wang, D. Pei, H. Fang, S. Zhong, H. Liu, J. Zhang, L. Tong, Y. Chen, Z. Li, M. H. Rümmeli, K. S. Novoselov, H. Peng, L. Lin, and Z. Liu, Nat. Commun. **12**, 2391 (2021).
129 G. Li, A. Luican, J. M. B. Lopes Dos Santos, A. H. Castro Neto, A. Reina, J. Kong, and E. Y. Andrei, Nat. Phys. **6**, 109 (2010), arXiv: 0912.2102.
130 G. Trambly de Laissardière, D. Mayou, and L. Magaud, Nano Lett. **10**, 804 (2010), arXiv: 0904.1233.
131 C. R. Dean, A. F. Young, I. Meric, C. Lee, L. Wang, S. Sorgenfrei, K. Watanabe, T. Taniguchi, P. Kim, K. L. Shepard, and J. Hone, Nat. Nanotech. **5**, 722 (2010), arXiv: 1005.4917.
132 L. Chen, L. He, H. S. Wang, H. Wang, S. Tang, C. Cong, H. Xie, L. Li, H. Xia, T. Li, T. Wu, D. Zhang, L. Deng, T. Yu, X. Xie, and M. Jiang, Nat. Commun. **8**, 14703 (2017), arXiv: 1703.03145.
133 F. Forster, A. Molina-Sanchez, S. Engels, A. Epping, K. Watanabe, T. Taniguchi, L. Wirtz, and C. Stampfer, Phys. Rev. B **88**, 085419 (2013), arXiv: 1212.3993.
134 X. Song, J. Gao, Y. Nie, T. Gao, J. Sun, D. Ma, Q. Li, Y. Chen, C. Jin, A. Bachmatiuk, M. H. Rümmeli, F. Ding, Y. Zhang, and Z. Liu, Nano Res. **8**, 3164 (2015).
135 J. Li, Y. Li, J. Yin, X. Ren, X. Liu, C. Jin, and W. Guo, Small **12**, 3645 (2016).
136 L. Wang, X. Xu, L. Zhang, R. Qiao, M. Wu, Z. Wang, S. Zhang, J. Liang, Z. Zhang, Z. Zhang, W. Chen, X. Xie, J. Zong, Y. Shan, Y. Guo, M. Willinger, H. Wu, Q. Li, W. Wang, P. Gao, S. Wu, Y. Zhang, Y. Jiang, D. Yu, E. Wang, X. Bai, Z. J. Wang, F. Ding, and K. Liu, Nature **570**, 91 (2019).
137 J. S. Lee, S. H. Choi, S. J. Yun, Y. I. Kim, S. Boandoh, J. H. Park, B. G. Shin, H. Ko, S. H. Lee, Y. M. Kim, Y. H. Lee, K. K. Kim, and S. M. Kim, Science **362**, 817 (2018).
138 S. M. Kim, A. Hsu, M. H. Park, S. H. Chae, S. J. Yun, J. S. Lee, D. H. Cho, W. Fang, C. Lee, T. Palacios, M. Dresselhaus, K. K. Kim, Y. H. Lee, and J. Kong, Nat. Commun. **6**, 8662 (2015).
139 Z. Shi, X. Wang, Q. Li, P. Yang, G. Lu, R. Jiang, H. Wang, C. Zhang, C. Cong, Z. Liu, T. Wu, H. Wang, Q. Yu, and X. Xie, Nat. Commun. **11**, 849 (2020).
140 T. A. Chen, C. P. Chuu, C. C. Tseng, C. K. Wen, H. S. P. Wong, S. Pan, R. Li, T. A. Chao, W. C. Chueh, Y. Zhang, Q. Fu, B. I. Yakobson, W. H. Chang, and L. J. Li, Nature **579**, 219 (2020), arXiv: 2105.15040.
141 D. Geng, X. Zhao, K. Zhou, W. Fu, Z. Xu, S. J. Pennycook, L. K. Ang, and H. Y. Yang, Adv. Mater. Interfaces **6**, 1801493 (2019).
142 G. H. Lee, Y. J. Yu, C. Lee, C. Dean, K. L. Shepard, P. Kim, and J. Hone, Appl. Phys. Lett. **99**, 243114 (2011).
143 K. K. Kim, A. Hsu, X. Jia, S. M. Kim, Y. Shi, M. Dresselhaus, T. Palacios, and J. Kong, ACS Nano **6**, 8583 (2012).
144 Q. H. Wang, K. Kalantar-Zadeh, A. Kis, J. N. Coleman, and M. S. Strano, Nat. Nanotech. **7**, 699 (2012).
145 K. F. Mak, K. L. McGill, J. Park, and P. L. McEuen, Science **344**, 1489 (2014), arXiv: 1403.5039.
146 C. Jin, J. Kim, M. I. B. Utama, E. C. Regan, H. Kleemann, H. Cai, Y. Shen, M. J. Shinner, A. Sengupta, K. Watanabe, T. Taniguchi, S. Tongay, A. Zettl, and F. Wang, Science **360**, 893 (2018).
147 Y. H. Lee, X. Q. Zhang, W. Zhang, M. T. Chang, C. T. Lin, K. D. Chang, Y. C. Yu, J. T. W. Wang, C. S. Chang, L. J. Li, and T. W. Lin, Adv. Mater. **24**, 2320 (2012).
148 Y. Gao, Y. L. Hong, L. C. Yin, Z. Wu, Z. Yang, M. L. Chen, Z. Liu, T. Ma, D. M. Sun, Z. Ni, X. L. Ma, H. M. Cheng, and W. Ren, Adv. Mater. **29**, 1700990 (2017).
149 J. Zhou, J. Lin, X. Huang, Y. Zhou, Y. Chen, J. Xia, H. Wang, Y. Xie, H. Yu, J. Lei, D. Wu, F. Liu, Q. Fu, Q. Zeng, C. H. Hsu, C. Yang, L. Lu, T. Yu, Z. Shen, H. Lin, B. I. Yakobson, Q. Liu, K. Suenaga, G. Liu, and Z. Liu, Nature **556**, 355 (2018).
150 P. Yang, X. Zou, Z. Zhang, M. Hong, J. Shi, S. Chen, J. Shu, L. Zhao, S. Jiang, X. Zhou, Y. Huan, C. Xie, P. Gao, Q. Chen, Q. Zhang, Z. Liu, and Y. Zhang, Nat. Commun. **9**, 979 (2018).
151 H. Yu, M. Liao, W. Zhao, G. Liu, X. J. Zhou, Z. Wei, X. Xu, K. Liu, Z. Hu, K. Deng, S. Zhou, J. A. Shi, L. Gu, C. Shen, T. Zhang, L. Du, L. Xie, J. Zhu, W. Chen, R. Yang, D. Shi, and G. Zhang, ACS Nano **11**, 12001 (2017).
152 J. Wang, X. Xu, T. Cheng, L. Gu, R. Qiao, Z. Liang, D. Ding, H. Hong, P. Zheng, Z. Zhang, Z. Zhang, S. Zhang, G. Cui, C. Chang, C. Huang, J. Qi, J. Liang, C. Liu, Y. Zuo, G. Xue, X. Fang, J. Tian, M. Wu, Y. Guo, Z. Yao, Q. Jiao, L. Liu, P. Gao, Q. Li, R. Yang, G. Zhang, Z. Tang, D. Yu, E. Wang, J. Lu, Y. Zhao, S. Wu, F. Ding, and K. Liu, Nat. Nanotechnol. **17**, 33 (2022).
153 L. Liu, T. Li, L. Ma, W. Li, S. Gao, W. Sun, R. Dong, X. Zou, D. Fan, L. Shao, C. Gu, N. Dai, Z. Yu, X. Chen, X. Tu, Y. Nie, P. Wang, J. Wang, Y. Shi, and X. Wang, Nature **605**, 69 (2022).
154 Y. Zuo, C. Liu, L. Ding, R. Qiao, J. Tian, C. Liu, Q. Wang, G. Xue, Y. You, Q. Guo, J. Wang, Y. Fu, K. Liu, X. Zhou, H. Hong, M. Wu, X. Lu, R. Yang, G. Zhang, D. Yu, E. Wang, X. Bai, F. Ding, and K. Liu, Nat. Commun. **13**, 1007 (2022).
155 Q. Wang, N. Li, J. Tang, J. Zhu, Q. Zhang, Q. Jia, Y. Lu, Z. Wei, H. Yu, Y. Zhao, Y. Guo, L. Gu, G. Sun, W. Yang, R. Yang, D. Shi, and G. Zhang, Nano Lett. **20**, 7193 (2020).
156 T. Li, W. Guo, L. Ma, W. Li, Z. Yu, Z. Han, S. Gao, L. Liu, D. Fan, Z. Wang, Y. Yang, W. Lin, Z. Luo, X. Chen, N. Dai, X. Tu, D. Pan, Y. Yao, P. Wang, Y. Nie, J. Wang, Y. Shi, and X. Wang, Nat. Nanotechnol. **16**, 1201 (2021).
157 S. H. Choi, H. J. Kim, B. Song, Y. I. Kim, G. Han, H. T. T. Nguyen, H. Ko, S. Boandoh, J. H. Choi, C. S. Oh, H. J. Cho, J. W. Jin, Y. S. Won, B. H. Lee, S. J. Yun, B. G. Shin, H. Y. Jeong, Y. M. Kim, Y. K. Han, Y. H. Lee, S. M. Kim, and K. K. Kim, Adv. Mater. **33**, 2006601 (2021).
158 H. Ye, J. Zhou, D. Er, C. C. Price, Z. Yu, Y. Liu, J. Lowengrub, J. Lou, Z. Liu, and V. B. Shenoy, ACS Nano **11**, 12780 (2017).
159 Q. Wang, J. Tang, X. Li, J. Tian, J. Liang, N. Li, D. Ji, L. Xian, Y. Guo, L. Li, Q. Zhang, Y. Chu, Z. Wei, Y. Zhao, L. Du, H. Yu, X. Bai, L. Gu, K. Liu, W. Yang, R. Yang, D. Shi, and G. Zhang, Natl. Sci. Rev. **9**, 6 (2022).